Journal of Zhejiang University-SCIENCE B 2025 26(10):1015-1036
www.jzus.zju.edu.cn; www.springer.com/journal/11585
E-mail: jzus_b@zju.edu.cn

Research Article
https://doi.org/10.1631/jzus.B2500154

Alamandine inhibits pathological retinal neovascularization by targeting the MrgD-mediated HIF-1α/VEGF pathway

Kun ZHAO[1*], Yaping JIANG[2*], Wen HUANG[1], Yukang MAO[1,3], Yihui CHEN[2], Peng LI[1✉], Chuanxi YANG[4✉]

[1]*Department of Cardiology, The First Affiliated Hospital with Nanjing Medical University, Nanjing 210029, China*
[2]*Department of Ophthalmology, Yangpu Hospital, Tongji University School of Medicine, Shanghai 200082, China*
[3]*Department of Cardiology, The Affiliated Suzhou Hospital of Nanjing Medical University, Suzhou 215000, China*
[4]*Department of Cardiology, Yangpu Hospital, Tongji University School of Medicine, Shanghai 200082, China*

Abstract: Retinopathy of prematurity (ROP) is a vision-threatening disorder that leads to pathological growth of the retinal vasculature due to hypoxia. Here, we investigated the potential effects of alamandine, a novel heptapeptide in the renin-angiotensin system (RAS), on hypoxia-induced retinal neovascularization and its underlying mechanisms. In vivo, the C57BL/6J mice with oxygen-induced retinopathy (OIR) were injected intravitreally with alamandine (1.0 μmol/kg per eye). In vitro, human retinal microvascular endothelial cells (HRMECs) were utilized to investigate the effects of alamandine (10 μg/mL) on proliferation, apoptosis, migration, and tubular formation under vascular endothelial growth factor (VEGF) stimulation. Single-cell RNA sequencing (scRNA-seq) matrix data from the Gene Expression Omnibus (GEO) database and RAS-related genes from the Molecular Signatures Database (MSigDB) were sourced for subsequent analyses. By integrating scRNA-seq data across multiple species, we identified that RAS-associated endothelial cell populations were highly related to retinal neovascularization. The liquid chromatography-tandem mass spectrometry (LC-MS/MS) analysis revealed a significant decrease in alamandine levels in both the serum and retina of OIR mice compared to those in the control group. Next, alamandine ameliorated hypoxia-induced retinal pathological neovascularization and physiologic revascularization in OIR mice. In vitro, alamandine effectively mitigated VEGF-induced proliferation, scratch wound healing, and tube formation of HRMECs primarily by inhibiting the hypoxia-inducible factor-1α (HIF-1α)/VEGF pathway. Further, coincubation with D-Pro[7] (Mas-related G protein-coupled receptor D (MrgD) antagonist) hindered the beneficial impacts of alamandine on hypoxia-induced pathological angiogenesis both in vivo and in vitro. Our findings suggested that alamandine could mitigate retinal neovascularization by targeting the MrgD-mediated HIF-1α/VEGF pathway, providing a potential therapeutic agent for OIR prevention and treatment.

Key words: Alamandine; Pathological neovascularization; Retinopathy of prematurity (ROP); Oxygen-induced retinopathy (OIR); Mas-related G protein-coupled receptor D (MrgD); Vascular endothelial growth factor (VEGF)

1 Introduction

Retinopathy of prematurity (ROP) is a vision-threatening disorder of multifactorial etiology that progresses to hypoxia-induced pathological growth of the retinal vasculature, resulting in permanent damage to the retina in preterm infants (Sabri et al., 2022). As a biphasic disease, ROP is initiated by oxygen therapy-induced delayed growth and degeneration of existing incomplete retinal blood vessels at birth, followed by the neovascularization of the retina and vitreous caused by the relatively hypoxic microvascular environment that cannot enable the adequate perfusion of avascular areas (Dammann et al., 2023). The presence of hypoxia-induced hypoxia-inducible factor-1α (HIF-1α)-dependent vascular endothelial growth factor (VEGF) stimulation predisposes vascular pathological changes, such as vascular leakage, vitreous hemorrhage, and angiogenesis, ultimately leading to retinal detachment and blindness in ROP (Broxterman and Hug, 2016).

✉ Peng LI, lipeng198610@163.com
Chuanxi YANG, 2205515@tongji.edu.cn
* The two authors contributed equally to this work
Peng LI, https://orcid.org/0000-0003-0365-2103
Chuanxi YANG, https://orcid.org/0000-0002-6970-1214

Received Mar. 27, 2025; Revision accepted May 15, 2025;
Crosschecked Sept. 25, 2025; Published online Oct. 7, 2025

Retinal hypoxia has been identified as the major stimulus that triggers pathological retinal neovascularization (RNV) in the development of ROP (Fevereiro-Martins et al., 2023). HIF-1, the oxygen-sensitive transcriptional activator, can orchestrate the process of angiogenesis by indirect cascade effects or direct binding to hypoxia-response element (HRE) sites in the promoters of HIF-1 target encoding genes like *vegf* (Zimna and Kurpisz, 2015). Under hypoxic conditions, the continuous accumulation of stabilized HIF-1α could translocate into the nucleus and then activate the transcriptional transactivation of proangiogenic genes, while VEGF is the most potent promoter involved in angiogenesis among them (Rattner et al., 2019). Additionally, VEGF can also be secreted by hypoxia-induced microglial cells in the vitreous, contributing to the resultant disordered angiogenesis in the ROP (Rathi et al., 2017). Hence, VEGF has been widely studied as a potential therapeutic target for retinal pathological angiogenesis (Uemura et al., 2021).

At present, laser and sometimes cryotherapy are considered for treatment-warranted ROP, but they cause permanent retinal destruction (Mintz-Hittner et al., 2011). Additionally, intravitreal injections of the VEGF inhibitor bevacizumab have been reported to improve ROP (Chang et al., 2022). As the upstream master regulatory gene for VEGF, there are currently few effective therapeutics targeting HIF-1α activity available (Xu et al., 2018). Thus, given that hypoxia-induced activation of HIF-1α is an important cause of abnormal neovascularization in hypoxic retinal diseases (Rattner et al., 2019), it is necessary to develop safe and valuable therapeutics for HIF-1α activity.

The pathogenetic actions of the renin-angiotensin system (RAS) have been evidenced to result in progressive alterations of various retinal vascular and neuro-glial diseases (Phipps et al., 2019). Angiotensin-(1–7) (Ang-(1–7)), a breakdown peptide hydrolyzed from Ang II, has been identified to inhibit the angiogenesis of various kinds of cancers by decreasing VEGF expression and attenuating hypoxia-stimulated cardiomyocyte apoptosis by inhibiting HIF-1α nuclear translocation (Chang et al., 2016; Domińska et al., 2018). As a novel vasoactive heptapeptide, alamandine, directly generated from the decarboxylation of Ang-(1–7) (Lautner et al., 2013), was considered to share similar molecular sequence and biological properties with Ang-(1–7) by activating Mas-related G protein-coupled receptor D (MrgD) (Zhao et al., 2022a). Recently, expression of MrgD receptors found in the retinal vasculature has also been reported to play a vital role in the retinal neurovascular function (Zhu et al., 2020). However, it remains unknown whether alamandine could inhibit neovascularization in OIR.

Thus, in our study, we aimed to investigate the anti-angiogenic effects of alamandine on hypoxia-induced RNV and to further explore its occurrence mechanisms.

2 Materials and methods

2.1 Analysis of single-cell transcriptomic data

Single-cell RNA sequencing (scRNA-seq) matrix data mainly from isolated retinal cells were obtained from Gene Expression Omnibus (GEO) database (GSE283276, GSE173079, GSE243100, and GSE150703), and scRNA-seq matrix data of fibrous membrane from proliferative vitreoretinopathy (PVR) or proliferative diabetic retinopathy (PDR) patients were obtained from GEO database (GSE165784 and GSE245561) for further analysis (Hu et al., 2022). RAS-related gene set (GO: 0003081) was sourced from the Molecular Signatures Database (MSigDB). A comprehensive set of 25 *Homo sapiens* genes and 36 *Mus musculus* genes was retrieved for subsequent analyses. Then, the Seurat package was used to conduct data analysis. Briefly, after mitigating batch effects and data normalization, uniform manifold approximation and projection (UMAP) was used to visualize and identify refined cell clusters. The cell types were identified by established marker genes in different cell clusters.

2.2 Animal care

This study used C57BL/6J female mice and their pups (regardless of gender) purchased from the Vital River Corporation (Beijing, China). Mice were housed on a circadian 12-h light–dark cycle (lights on at 07:00 am and off at 07:00 pm) and were permitted free access to food and water.

2.3 Animal model and treatment protocols

The mouse models of oxygen-induced retinopathy (OIR) are reproducible and quantifiable in terms

of observing the progression of RNV, making it a good model for mimicking ROP and examining the occurrence mechanisms underlying its pathogenesis (Rivera et al., 2016).

Newborn C57Bl/6J mice at postnatal Day 7 (P7) were exposed to 75% (volume fraction) oxygen for five consecutive days along with their mothers and were then returned to normal conditions (21% oxygen) from P12 to P17. Next, the retinas from OIR mice at P17 were obtained for further experiments.

2.4 Intravitreal injections

First, 0.5 μL alamandine (1.0 μmol/kg (Li et al., 2018); Synpeptide Co., Ltd., Shanghai, China) diluted in phosphate-buffered saline (PBS) was intravitreally injected using a 33-G needle and Hamilton syringe into each eye of the mice at P12. In another experiment, 0.5 μL D-Pro^7-Ang-(1–7) (D-Pro^7; 1 μmol/L (Yang et al., 2020); Bachem, CA, USA) or A779 (10 μmol/L (Yang et al., 2020); Bachem) was intravitreally injected 3 h before alamandine. PBS was used as a control.

2.5 Immunofluorescent staining

Flat mounts of the P17 retina were prepared according to the approach (Tual-Chalot et al., 2013). Concisely, both eyes were enucleated from euthanized neonatal mice and immersed in 4% (0.04 g/mL) paraformaldehyde (PFA) for 15 min at room temperature. Then, the retinas were carefully separated from surrounding tissues, radially cut using microscissors, and treated with cold methanol for 20 min or longer. Once the procedures above were finished, the retinas were washed gently with PBS containing 0.1% (volume fraction) Tween-20, blocked with blocking solution containing 5% (0.05 g/mL) goat serum and 0.3% (volume fraction) TritonX-100 diluted in PBS for 2 h at room temperature, and probed with fluorescein-tagged isolectin B4 (IB4; 1:150 (volume ratio) diluted in blocking solution) overnight at 4 °C. After rinsing with PBS for three times, sections were mounted on Superfrost Plus slides, air-dried, and coverslipped with antifade mounting medium containing 4',6-diamidino-2-phenylindole (DAPI) (Vector Laboratories, Burlingame, CA, USA). All fluorescence images were captured by a confocal laser scanning microscope (Carl Zeiss, Oberkochen, Germany).

2.6 Quantitation of retinal neovascularization in OIR mice

Retinal vaso-obliteration (RVO) and RNV were quantitatively analyzed as previously described (Zhao et al., 2022b). Briefly, the retinal whole-mount was stained with IB4 to label endothelial cells. Then, the images of whole-mount retinas were taken using a Zeiss fluorescence upright microscope (Carl Zeiss, Jena, Germany). Next, we quantified RVO and RNV by comparing the number of pixels in a given region to the total number of retinal pixels in images of whole-mount retinas of mice from different groups via ImageJ software (The National Institute of Health, Bethesda, MD, USA). The new vessels that fluoresced more intensely than the surrounding normal vessels would be colored red (Connor et al., 2009).

2.7 Culture and treatment of human retinal microvascular endothelial cells

Human retinal microvascular endothelial cells (HRMECs) (Angio-Proteomie, Boston, MA, USA; CAP-0010) were cultured in endothelial cell medium (ECM) (ScienCell, Carlsbad, CA, USA) at 37 °C with 5% CO_2. To mimic the OIR model in vitro, HRMECs at passages five or six were placed in a homemade hypoxia incubator filled with 1% O_2, 5% CO_2, and 94% N_2 for 24 h, as previously reported (Ahmed et al., 2016). In some experiments, HRMECs were preliminarily incubated with alamandine (5, 10, and 20 μg/mL), D-Pro^7 (1 μmol/L), or A779 (10 μmol/L) for 30 min before hypoxia treatment. In some experiments, HRMECs were treated with 1 μmol/L Ang II for 48 h to induce a pathological model. All the cells were then subjected to the following studies.

2.8 Wound healing assay

To decipher the impact of alamandine on cell migration capacity, HRMECs were cultured on 6-well plates before reaching a confluence of 90%. A pipette tip was utilized to artificially generate a straight wound. Live cell images were collected 24 h after varying concentrations of alamandine administration by a bright-field microscope and were processed with ImageJ software to calculate the wound width. A shorter width is routinely the consequence of a better migration rate of HRMECs.

2.9 Real-time cell analyzer proliferation and migration assays

A cell analyzer system constructed upon electrical impedance measurement offers a real-time means for recording the extent to which alamandine alters the proliferation and migration status of HRMECs. To monitor the proliferation process, cells (2×10^3 per well) were seeded in an E-plate 16 (ACEA Biosciences, San Diego, USA), and 8 h later, the cell suspension was transferred to serum-free medium with/without 10 ng/mL VEGF, with alamandine being added at various concentrations. As for the migration assay, cells were seeded in a CIM-plate 16 (xCELLigence Roche, Penzberg, Germany) containing a serum-free medium. Each well of the lower chamber was filled with a certain concentration of alamandine and 10 ng/mL VEGF to elicit chemotactic migration.

2.10 Aortic ring angiogenesis assay

The procedures for detecting ex vivo aortic angiogenesis with the Sprague-Dawley rats' aorta in our study were identical to previously established protocols (Nicosia and Ottinetti, 1990). After sacrifice, the thoracic aorta of rats was completely isolated and cut into 1 mm rings. Having been embedded in a 96-well plate (Corning, NY, USA) coated with Matrigel matrix, the aortic rings were then maintained in M119 medium supplemented with 2% (volume fraction) fetal bovine serum (FBS), VEGF (10 ng/mL), and alamandine for 6 d. During this period, we renewed the growth medium at 2-d intervals. The degree of angiogenic sprouting from the aortic rings was microscopically inspected and photographed with a 10× objective, manually analyzed, and assigned a score ranging from 0 (least evident) to 5 (most evident) by a blinded investigator.

2.11 Tube formation assay for HRMECs

In vitro tube formation assay was conducted using a commercial tube formation kit (Cultrex, USA) following the manufacturer's guidance. HRMECs (2×10^4 per well) were seeded in Matrigel matrix-coated 24-well plates (100 μL/well). The cumulative amount and length of the tube were quantified with the assistance of ImageJ software.

2.12 Flow cytometry

The collected viable cells and cell debris were incubated with propidium iodide (PI) and Annexin-V (Fcmacs Biotech Co., China) in the binding buffer at room temperature for 30 min in darkness according to the manufacturer's instructions. Then, the flow cytometry method was applied to analyze the relative ratio of cell apoptosis.

2.13 Nuclear protein extraction

The nuclear protein was extracted using the NucBuster™ Protein Extraction Kit (Novagen®, Rockland, DE, USA), according to the manufacturer's protocol.

2.14 Western blotting

The total proteins of HRMECs and retinas were isolated with radioimmunoprecipitation (RIPA) lysis buffer (containing phosphatase and protease inhibitor cocktails), with the protein concentration being measured using the bicinchoninic acid (BCA) Protein Assay Kit (Pierce, Rockford, IL, USA). Approximately 30–50 μg of protein from each sample was loaded for 10% (0.01 g/mL) sodium dodecyl sulfate-polyacrylamide gel electrophoresis (SDS-PAGE) and was subsequently transferred onto polyvinylidene difluoride (PVDF) membranes (Millipore, Bedford, MA, USA). A 5% (0.05 g/mL) bovine serum albumin (BSA) solution was prepared for blocking non-specific binding. Membranes were incubated with primary antibodies overnight at 4 ℃, followed by incubation with horseradish peroxidase-conjugated secondary antibodies at room temperature for 2 h. After three washes with Tris-buffered saline with Tween-20 (TBST), protein bands were visualized with enhanced chemiluminescence reagent, with band densities being quantified using ImageJ software. To compare the protein levels among different samples, β-actin was used as an internal reference. Primary antibodies used were as follows: caspase 3 (1:1000 (volume ratio, the same as below), #14220; Cell Signaling Technology, MA, USA), cleaved caspase 3 (CC3) (1:1000, #9664; Cell Signaling Technology), B cell lymphoma-2 (Bcl-2)-associated X (Bax) (1:1000, #5023; Cell Signaling Technology), Bcl-2 (1:1000, #15071; Cell Signaling Technology), HIF-1α (#36169; Cell Signaling Technology), VEGF (No. 19003-1-AP; Proteintech Co., Wuhan, China), proliferating cell nuclear antigen (PCNA) (No. 10205-2-AP; Proteintech Co.), MrgD (1:1000; Abcam), endothelial nitric oxide synthase (eNOS) (1:1000, #32027; Cell Signaling Technology), and inducible nitric oxide synthase (iNOS) (No. 22226-1-AP; Proteintech Co.).

2.15 qRT-PCR

Total RNA extraction from cells or tissues was performed using the TRIzol™ reagent (Invitrogen, Carlsbad, CA, USA). After examining RNA concentration and purity using a NanoDrop-1000 spectrophotometer (Thermo Scientific, Wilmington, DE, USA), the PrimeScript™ RT Reagent Kit (TaKaRa Bio, Otsu, Japan) was applied for generating reverse-transcribed complementary DNA (cDNA). A SYBR green-based quantitative reverse transcription-polymerase chain reaction (qRT-PCR) assay was conducted on an ABI Prism 7000 sequence detection system (Applied Biosystems, Foster City, CA, USA) to detect messenger RNA (mRNA) expression. Relative gene expression was determined using the $2^{-\Delta\Delta C_T}$ method and was normalized to the internal control gene glyceraldehyde-3-phosphate dehydrogenase (*GAPDH*). For microRNA (miRNA) quantification, the BulgeLoop™ miRNA Reverse Transcription Kit (RiboBio, Guangzhou, China), the Bulge-Loop™ miRNA qRT-PCR Starter Kit (RiboBio, Guangzhou, China), and miRNA-specific primers (RiboBio, Guangzhou, China) were used, with *GAPDH* serving as an endogenous control. The primer sequences used in this study were illustrated item by item in Table 1.

2.16 Liquid chromatography-tandem mass spectrometry

We performed liquid chromatography-tandem mass spectrometry (LC-MS/MS) to identify the metabolites of the retinas or serum of the mice from the normoxia and hypoxia groups. First, we extracted the metabolites from the retinas via 80% (volume fraction) CH_3OH/Milli-Q water. Then, the dried samples were transferred to autosampler vials for LC-MS/MS analysis (n=6). Briefly, reversed-phase LC (HP1100, Agilent Technologies, Santa Clara, USA) was used to separate the metabolites. Next, each sample was injected into the C18 column for analysis. Finally, data analysis was performed using the XCMSOnline at https://xcmsonline.scripps.edu.

2.17 Statistical analysis

Data are expressed as mean±standard error of the mean (SEM). One-way analysis of variance (ANOVA) followed by Bonferroni's post hoc test was performed to evaluate the significance of multigroup mean differences. Values were considered statistically significant for P<0.05. All the data were analyzed using GraphPad Prism 7.0 software (GraphPad Inc., San Diego, USA).

Table 1 List of utilized primers for quantitative reverse transcription-polymerase chain reaction (qRT-PCR)

Gene	Species	Forward primer (5'→3')	Reverse primer (5'→3')
VEGF	Human	GCAGAAGGAGGAGGGCAG	CACCAGGGTCTCGATTGGAT
HIF-1α	Human	CGGAAACTGAAGACCAACAAC	CAGAGGCAGGTAATGGAGACA
IL-1β	Human	ATGATGGCTTATTACAGTGGCAA	GTCGGAGATTCGTAGCTGGA
IL-6	Human	ACTCACCTCTTCAGAACGAATTG	CCATCTTTGGAAGGTTCAGGTTG
TNF-α	Human	GAGGCCAAGCCCTGGTATG	CGGGCCGATTGATCTCAGC
MCP-1	Human	CTCAGCCAGATGCAGTTAATG	TCTCCAGCCGACTCATTGG
ICAM-1	Human	ATGCCCAGACATCTGTGTCC	GGGGTCTCTATGCCCAACAA
VCAM-1	Human	GGGAAGATGGTCGTGATCCTT	TCTGGGGTGGTCTCGATTTTA
MMP-9	Human	TGTACCGCTATGGTTACACTCG	GGCAGGGACAGTTGCTTCT
ACE	Human	GGGAAAGGCACTACCATGTCG	GGTGAGTTGTTGTCTGGCTTC
AGT	Human	TCCAGACTCCGATCATCAAGC	GCTCATGGTGTTCAGAATTGTGT
AT1	Human	CCCCAGTCTGAGATGGCTC	GACGAGGTGGAAGGGGTGTA
GAPDH	Human	GGAGCGAGATCCCTCCAAAAT	GGCTGTTGTCATACTTCTCATGG
Vegf	Mice	CTGCCGTCCGATTGAGACC	CCCCTCCTTGTACCACTGTC
Hif-1α	Mice	ACCTTCATCGGAAACTCCAAAG	CTGTTAGGCTGGGAAAAGTTAGG
Gapdh	Mice	CCTCGCCTTTGCCGATCC	GGATCTTCATGAGGTAGTCAGTC

VEGF: vascular endothelial growth factor; *HIF-1α*: hypoxia-inducible factor-1α; *IL*: interleukin; *TNF-α*: tumor necrosis factor-α; *MCP-1*: monocyte chemoattractant protein-1; *ICAM-1*: intercellular adhesion molecule-1; *VCAM-1*: vascular cellular adhesion molecule-1; *MMP-9*: matrix metallopeptidase-9; *ACE*: angiotensin-converting enzyme; *AGT*: angiotensinogen; *AT1*: alveolar epithelial type 1; *GAPDH*: glyceraldehyde-3-phosphate dehydrogenase.

3 Results

3.1 scRNA-seq data integration and clustering

We first integrated scRNA-seq data (including GSE165784 and GSE245561) of fibrous membrane from PVR or PDR patients via Harmoney, single-cell variational inference (scVI), and Seurat analysis methods (Fig. 1a). Based on the Seurat method, which provided the most competitive results, seven different color-coded cell types were annotated in Seurat UMAP clustering plot, and their proportions in the PDR and PVR samples were also represented in a bar graph (Fig. 1b). Next, a comprehensive gene set of 25 *H. sapiens* genes and 36 *M. musculus* genes, termed regulated alternative splicing genes (RASGs), was retrieved from the MSigDB database to investigate the possible relationship between RAS and PDR. The average gene expression of RASGs in distinct cell types was visualized in a heatmap, Violin plot, and UMAP clustering plot (Figs. 1c–1e). The results showed that RASGs were expressed at highest levels in the subsets of microglial cells and endothelial cells (ECs). Considering the reported value of ECs in the development of pathological RNV (Huang, 2020), we further clustered EC subset into six subclusters (VEC1–6) to explore their distribution pattern (Fig. 1f). The subclusters were scored in accordance with RASG expression, and their gene expression profiles were showed in Figs. 1g and 1h. Furthermore, we integrated scRNA-seq data (including GSE283276, GSE173079, GSE243100, and GSE150703) of isolated retinal cells from OIR, PDR, and control mouse models. The Seurat UMAP clustering plot showed 12 different color-coded cell types (Figs. 2a and 2b). The average gene expression of RASGs in distinct cell types was also visualized (Figs. 2c–2e), and the expression of RASGs was highest in the subsets of microglial cells, ECs, and pericyte cells. The gene expression profiles of five subclusters scored according to RASG expression were shown in Figs. 2f–2h. By integrating transcriptomic data across multiple species, we identified that RAS-associated EC populations were indeed highly related to RNV, establishing a foundation for developing targeted therapeutic strategies that modulate RAS activity to mitigate pathological neovascularization. Thus, we further explored the possible role of RAS in EC dysfunction.

3.2 LC-MS/MS-mediated metabolomics analysis of the OIR mouse model

To explore the occurrence mechanisms of ROP, we first established the OIR mouse model in vivo. Then, based on the role of the high-throughput LC-MS/MS method in revealing mechanisms and therapeutic targets for different diseases, we performed the LC-MS/MS method to qualitatively analyze the different compounds of the RAS in serum and retina tissues between the OIR and control groups to explore the novel mechanisms of ROP development. The results showed that the heptapeptide alamandine in serum and retinas is significantly decreased in OIR mice compared with the control group (Figs. 3a and 3b).

Alamandine, generated from catalytic hydrolysis of Ang A via angiotensin-converting enzyme 2 (ACE2), is a novel member involved in the ACE2/Ang-(1–7)/Mas protective axis in the RAS. Due to the different expression of alamandine in serum and retinas between the OIR and control groups, we next detected some other vital RAS members that are involved in the generation of alamandine. Compared with the control group, our analysis of LC-MS/MS data in the OIR group showed higher levels of Ang II (Figs. 3c and 3d) and lower levels of ACE2 (Figs. 3e and 3f) in serum and retinas. Moreover, *ACE*, angiotensinogen (*AGT*), and angiotensin II type 2 (*AT2*) mRNA expression levels were lower in hypoxia-induced HRMECs versus control (Fig. S1). The above LC-MS/MS results suggested that the expression of RAS members, especially the novel polypeptide alamandine, may be affected during the occurrence and progression of ROP. Considering that the expression of MrgD, the natural receptor of alamandine, has also recently been reported to play a crucial role in retinal neurovascular function (Zhu et al., 2020), we were eager to further explore the possible role of alamandine in the development of ROP.

3.3 Effects of alamandine on VEGF-induced angiogenesis in HRMECs

To investigate the potential values of alamandine in angiogenesis in vitro, further studies were conducted on VEGF-mediated angiogenesis in HRMECs. First, the results of flow cytometry showed that there was no statistical significance between different groups, meaning that different concentrations (5, 10, and 20 μg/mL)

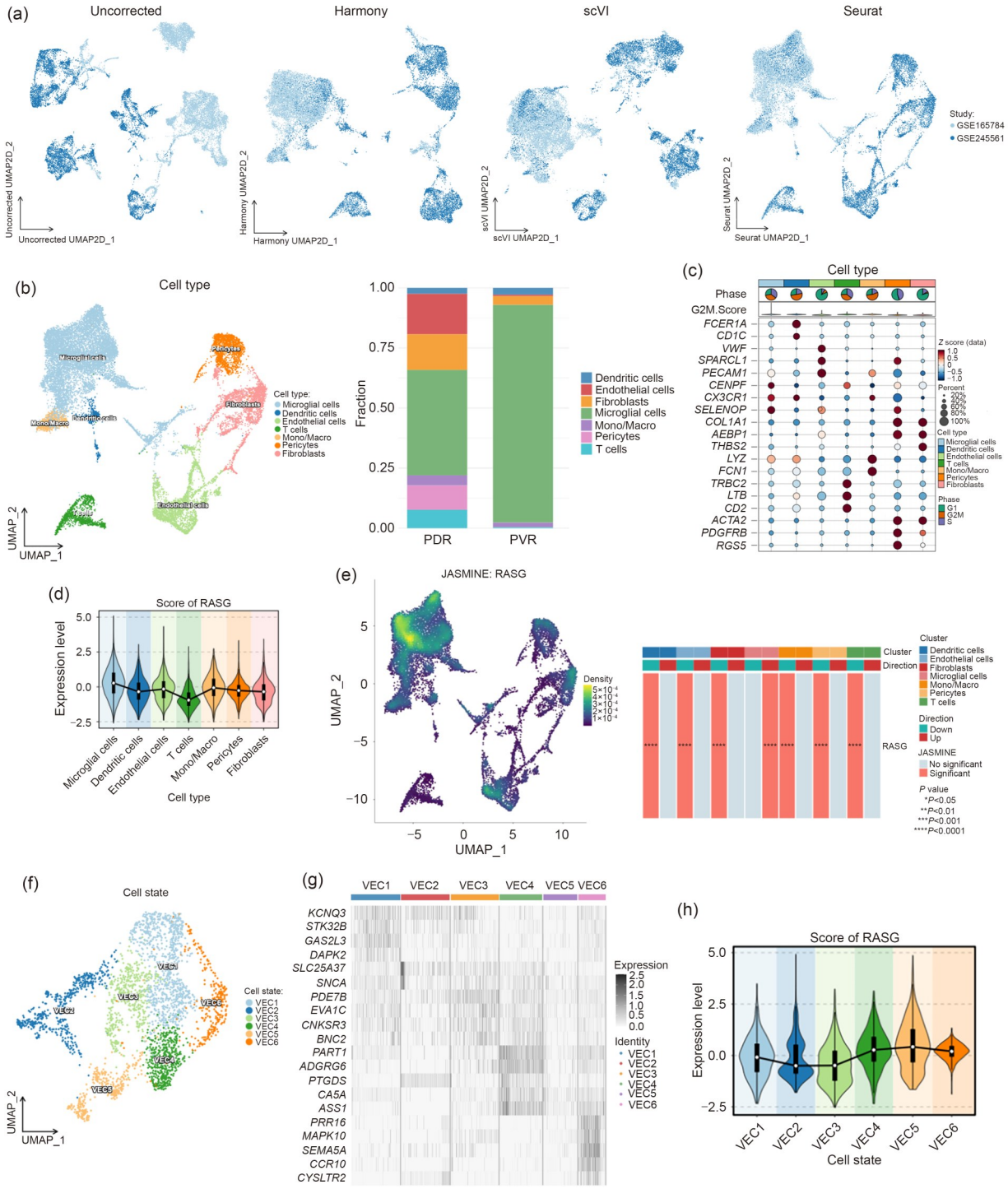

Fig. 1 Analysis of single-cell transcriptomic data in humans. (a) The uncorrected and three types of re-clustered uniform manifold approximation and projection (UMAP) clustering of single-cell transcriptomic data from Gene Expression Omnibus (GEO) datasets. (b) Seurat UMAP clustering of cell types (left) and its bar graph (right). (c) Heatmap of expression levels of renin-angiotensin system-related genes (RASGs) in key cell types of isolated retinal cells. (d) Violin plot of expression levels of RASGs in key cell types of isolated retinal cells from proliferative vitreoretinopathy (PVR) and proliferative diabetic retinopathy (PDR) patients. (e) UMAP of density scores of the RASGs in different cell types; and its visualized bar graph. (f) UMAP plots of six clusters (VEC1–6) in endothelial cells (ECs). (g) Heatmap of leading signature gene expression profiles for the six EC clusters; (h) Expression scores of RASGs in six EC clusters. scVI: single-cell variational inference.

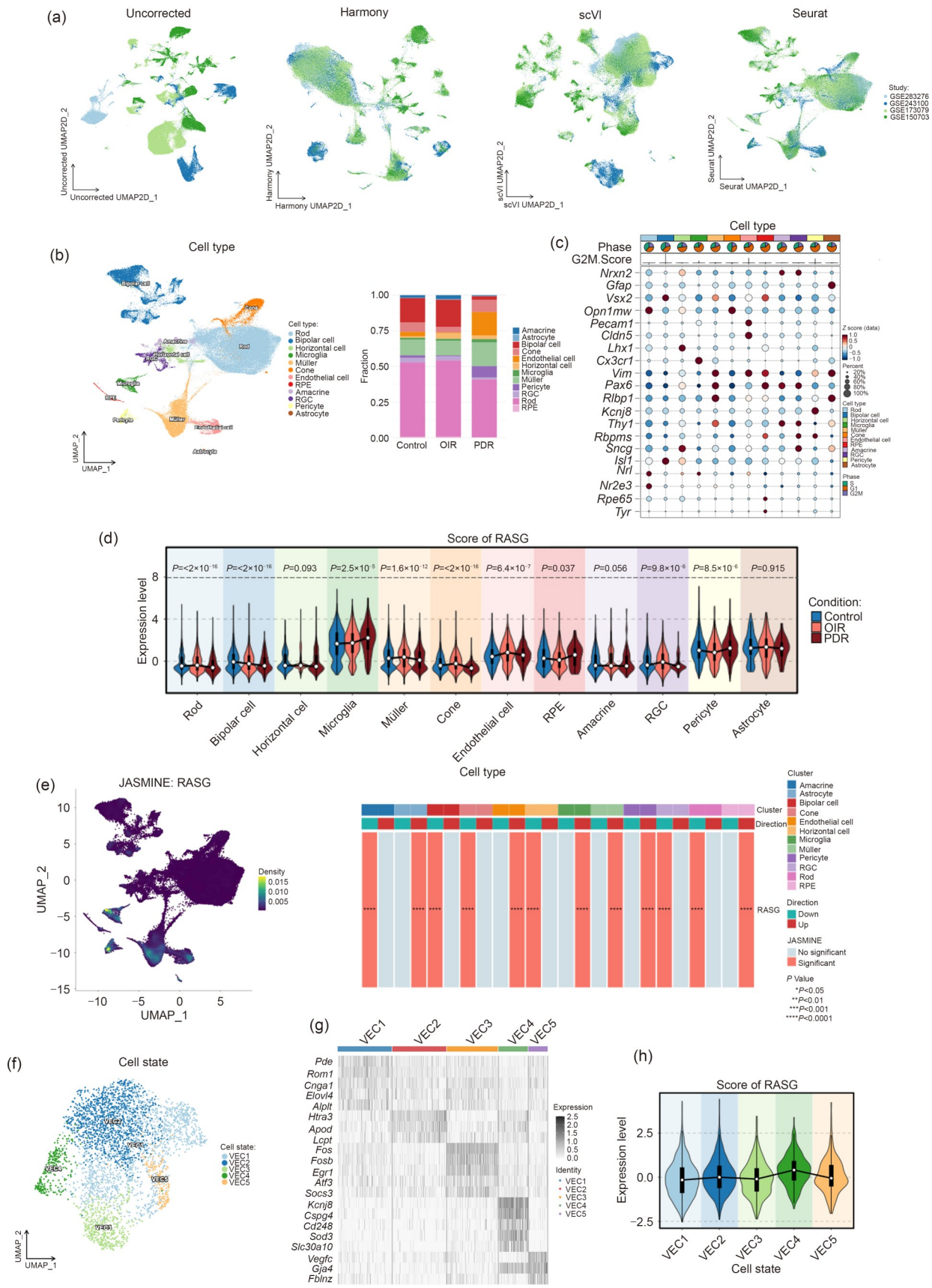
(a)
Uncorrected
Harmony
scVI
Seurat
Study:
GSE283276
GSE243100
GSE173079
GSE150703
(b)
Cell type
Rod
Bipolar cell
Horizontal cell
Microglia
Müller
Cone
Endothelial cell
RPE
Amacrine
RGC
Pericyte
Astrocyte
Fraction
Control
OIR
PDR
(c)
Cell type
Phase
G2M.Score
Nrxn2
Gfap
Vsx2
Opn1mw
Pecam1
Cldn5
Lhx1
Cx3cr1
Vim
Pax6
Rlbp1
Kcnj8
Thy1
Rbpms
Sncg
Isl1
Nrl
Nr2e3
Rpe65
Tyr
(d)
Score of RASG
Expression level
P=<2×10⁻¹⁶
P=<2×10⁻¹⁶
P=0.093
P=2.5×10⁻⁵
P=1.6×10⁻¹²
P=<2×10⁻¹⁶
P=6.4×10⁻⁷
P=0.037
P=0.056
P=9.8×10⁻⁶
P=8.5×10⁻⁶
P=0.915
Condition:
Control
OIR
PDR
(e)
JASMINE: RASG
Density
Cluster
Direction
RASG
Down
Up
No significant
Significant
(f)
Cell state
Cell state:
VEC1
VEC2
VEC3
VEC4
VEC5
(g)
Pde
Rom1
Cnga1
Elovl4
Alplt
Htra3
Apod
Lcpt
Fos
Fosb
Egr1
Atf3
Socs3
Kcnj8
Cspg4
Cd248
Sod3
Slc30a10
Vegfc
Gja4
Fblnz
Expression
Identity
(h)
Score of RASG
Expression level
Cell state

Fig. 2 Analysis of single-cell transcriptomic data in mice. (a) Uncorrected and three types of re-clustered uniform manifold approximation and projection (UMAP) clustering of single-cell transcriptomic data from Gene Expression Omnibus (GEO) datasets. (b) Seurat UMAP clustering of cell types (left) and its bar graph (right). (c) Heatmap of expression levels of renin-angiotensin system-related genes (RASGs) in key cell types of isolated retinal cells. (d) Violin plot of expression levels of RASGs in key cell types of isolated retinal cells from oxygen-induced retinopathy (OIR), proliferative diabetic retinopathy (PDR), or control mouse models. (e) UMAP of density scores of the RASGs in different cell types (left) and its visualized bar graph (right). (f) UMAP plots of five clusters (VEC1–5) in endothelial cells (ECs). (g) Heatmap of the leading signature gene expression profiles for the five EC clusters. (h) Expression scores of RASGs in five EC clusters. scVI: single-cell variational inference.

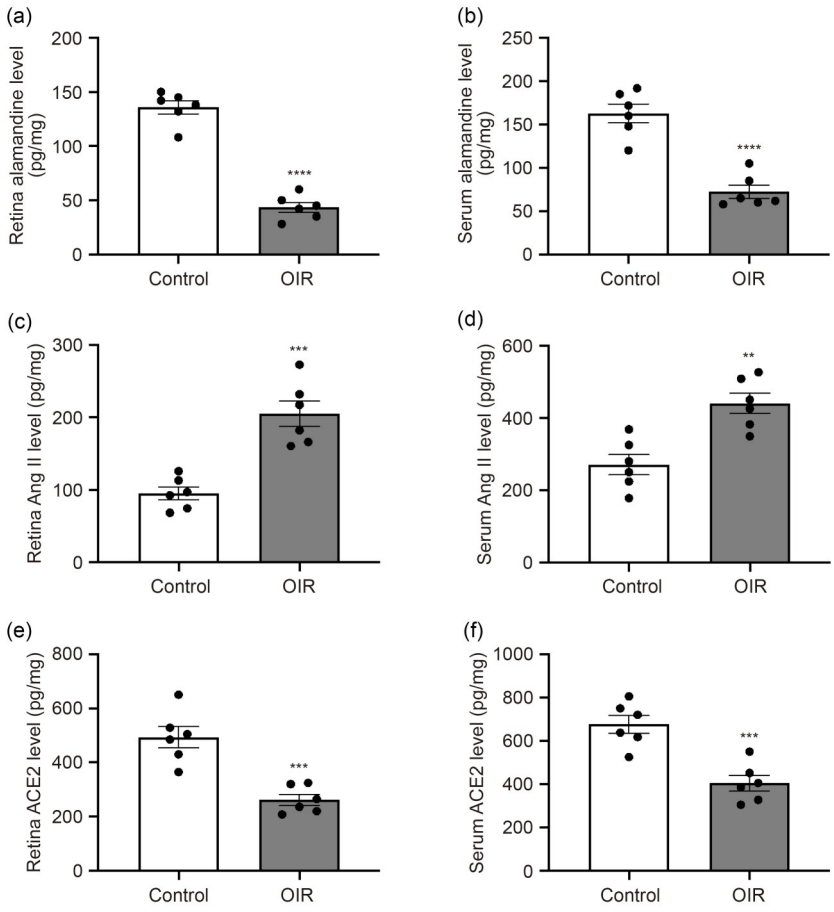

Fig. 3 Liquid chromatography-tandem mass spectrometry (LC-MS/MS)-mediated metabolomics analysis of oxygen-induced retinopathy (OIR) mouse model. (a, b) High-throughput LC-MS/MS qualitatively analyzed alamandine in retina (a) and serum (b) tissues between the OIR and control groups. (c–f) High-throughput LC-MS/MS qualitatively analyzed angiotensin II (Ang II) (c, d) and angiotensin-converting enzyme 2 (ACE2) (e, f) in retina (c, e) and serum (d, f) tissues between the OIR and control groups. All the results are expressed as mean±standard error of mean (SEM) (n=6 per group). ** P<0.01, *** P<0.001, **** P<0.0001, compared with the control group.

of alamandine have no evident pro-apoptotic effects on cultured HRMECs (Fig. 4a). Subsequent real-time cellular analysis (RTCA) showed that alamandine could significantly attenuate VEGF-induced EC migration and proliferation in a dose-dependent manner (Figs. 4b and 4c). Since pathological angiogenesis is characterized by EC migration, tube formation, and microvascular sprout induced by VEGF or a hypoxic microenvironment, wound healing assay, tube-formation assay, and aortic ring assay were further carried out to confirm the role of alamandine in ex vivo angiogenesis in HRMECs. As shown in Figs. 4d and 4e, alamandine could dose-dependently inhibit VEGF-induced closure of the scratch wound and capillary-like tube formation. In addition, the numbers and morphology of new growth sprouts surrounding the aortic rings showed that VEGF promoted microvascular sprouting and blood vessel network formation, which

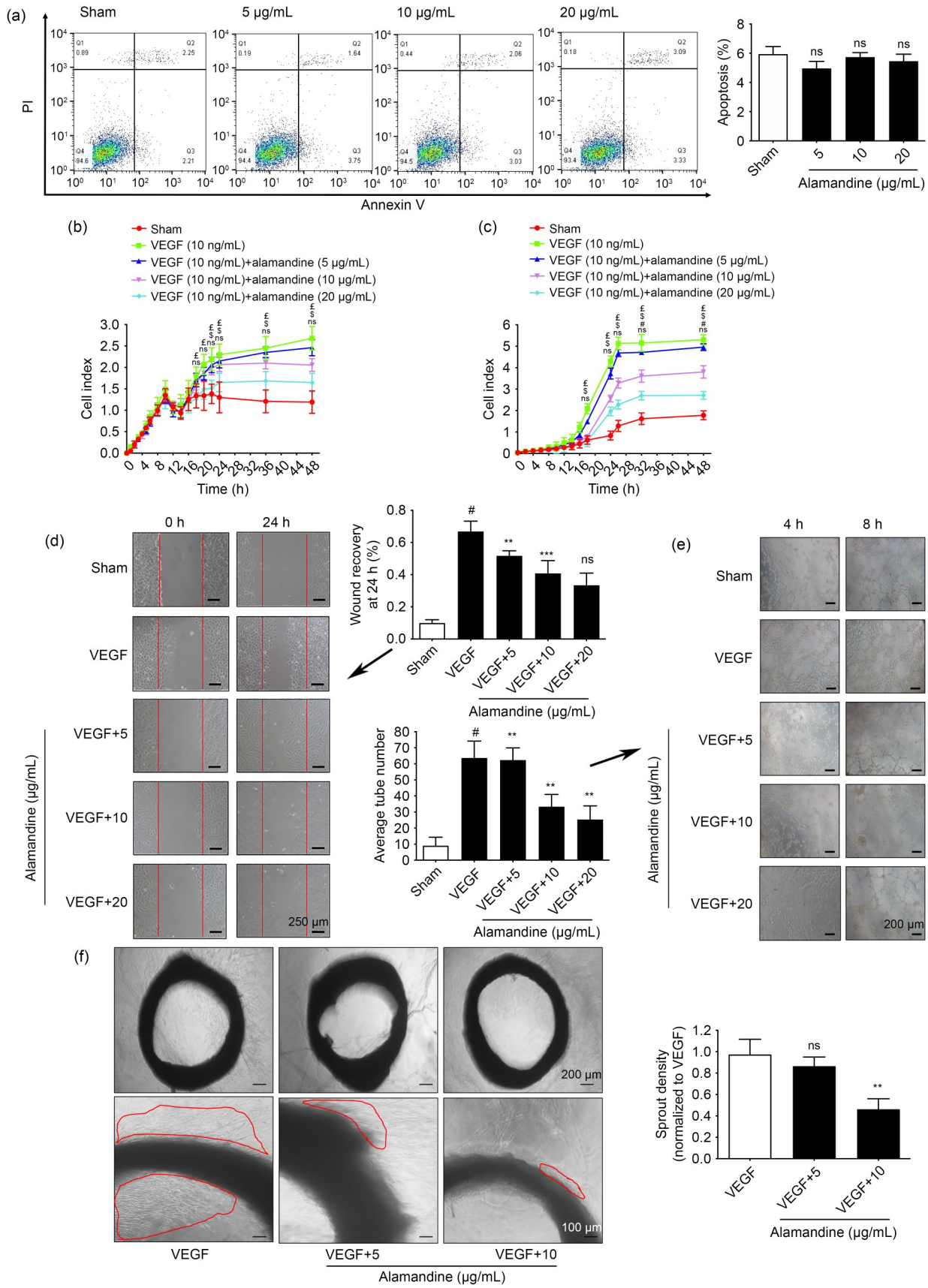
(a)
Sham
5 μg/mL
10 μg/mL
20 μg/mL
PI
Annexin V
Apoptosis (%)
Alamandine (μg/mL)
(b)
Sham
VEGF (10 ng/mL)
VEGF (10 ng/mL)+alamandine (5 μg/mL)
VEGF (10 ng/mL)+alamandine (10 μg/mL)
VEGF (10 ng/mL)+alamandine (20 μg/mL)
Cell index
Time (h)
(c)
(d)
0 h
24 h
Wound recovery at 24 h (%)
Alamandine (μg/mL)
250 μm
(e)
4 h
8 h
200 μm
Average tube number
(f)
200 μm
100 μm
Sprout density (normalized to VEGF)

Fig. 4 Effects of alamandine on vascular endothelial growth factor (VEGF)-induced angiogenesis in human retinal microvascular endothelial cells (HRMECs). (a) Flow cytometric analysis of apoptosis in HRMECs treated with different concentrations (5, 10, and 20 μg/mL) of alamandine (left) and its corresponding quantitative analysis (right). (b, c) Results of real-time cellular analysis (RTCA) migration (b) and proliferation (c) assays performed to determine the effects of different concentrations (5, 10, and 20 μg/mL) of alamandine on VEGF-induced migration and proliferation of HRMECs, respectively. ns: not significant; $^{\#,\$,\pounds}$ P<0.05, VEGF+5, 10, and 20 μg/mL alamandine group vs. VEGF group, respectively. (d–f) Results of wound healing assay (d), tube-formation assay (e), and aortic ring assay (f), which were performed to examine the role of alamandine in VEGF-induced angiogenesis in HRMECs. VEGF: 10 ng/mL. All the results are expressed as mean±standard error of mean (SEM) (n=5 per group). ns: not significant; ** P<0.01, *** P<0.001, compared with the VEGF group; $^{\#}$ P<0.001, compared with the sham group. PI: propidium iodide.

could be suppressed by alamandine treatment dose-dependently (Fig. 4f). We also found that alamandine ameliorated Ang II-induced EC apoptosis, migration, and proliferation (Fig. S2). Collectively, these results indicated that alamandine did prevent VEGF-induced angiogenesis in vitro.

3.4 Effects of alamandine on hypoxia-induced HIF-1α/VEGF pathway activation and apoptosis in HRMECs

Next, we investigated the expression of the HIF-1α/VEGF pathway, which has been reported to play a crucial role in continuous inflammatory infiltration involved in hypoxia-induced microvascular angiogenesis. As shown in Figs. 5a and 5b, hypoxia could increase mRNA expression of *VEGF* in HRMECs, and then 10 μg/mL alamandine was chosen as the most suitable concentration for further experiments. Next, the protein expression levels of HIF-1α, VEGF, and CC3, as well as the ratio of Bax/Bcl-2, were increased after 24 h of hypoxia induction in HRMECs; however, they were inhibited by alamandine treatment (Figs. 5c–5g). The above results suggested that alamandine could prevent hypoxia-induced apoptosis and activation of the HIF-1α/VEGF pathway in vitro, which could be supported by further immunofluorescence results of HRMEC staining with HIF-1α or CC3 (Figs. 5h–5k). The western blot results also showed that alamandine dramatically inhibited hypoxia-induced nuclear import of HIF-1α in vitro (Fig. 5l). Next, HIF-1α stabilizer dimethyloxalylglycine (DMOG) hindered the inhibitory effects of alamandine on hypoxia-induced VEGF and PCNA (Fig. 5m).

3.5 Effects of alamandine on pathological neovascularization in the retinas of OIR mice

To further investigate the role of alamandine in regulating RNV in OIR mouse models, retinal paraffin section staining with hematoxylin and eosin (H&E) and whole-mount immunostaining with IB4 were performed on P17 (Figs. 6a and 6b). As shown in the high-resolution images, the increased number of hypoxia-stimulated pre-retinal neovascular cell nuclei penetrating the internal limiting membrane (ILM) in the OIR group (labeled as hypoxia group in figures). was decreased by the alamandine treatment. Additionally, the percentages of neovascular tuft areas (Fig. 6c) and neovascular areas (Fig. 6d), as well as the ratio of avascular areas to total areas (Fig. 6e), were increased in mouse retinas from the OIR group compared with the control group, which were reduced after intravitreal injection of alamandine. Notably, alamandine alone has no significant adverse effects on retinal vessel development in a normal retina (Fig. S3). These data indicated that alamandine could dramatically improve hypoxia-induced retinal pathological neovascularization and physiologic revascularization in mouse models of OIR.

3.6 Effects of alamandine on vessel proliferation and HIF-1α/VEGF pathway activation in the retinas of OIR mice

Since hypoxia-induced VEGF favors angiogenesis and vasoproliferation, which can result in abnormal neovascularization (Rattner et al., 2019), we used PCNA as a proliferation marker to examine the proliferation capacity of vessel ECs in vivo. The OIR-induced protein expression of PCNA in retinas was significantly decreased by alamandine (Fig. 6f). In agreement with western blot results, the density of PCNA-positive cells was increased within the retinal neovessels in the OIR group compared with that in the control group, which was decreased after the administration of alamandine (Fig. 6g). Then, we examined whether the HIF-1α/VEGF pathway was also involved in the beneficial effects of alamandine in vivo. The same trend was found in the mRNA expression of *HIF-1α* (Fig. 6h) and *VEGF* (Fig. 6i) in vivo. Consistent with the above western blot and PCR

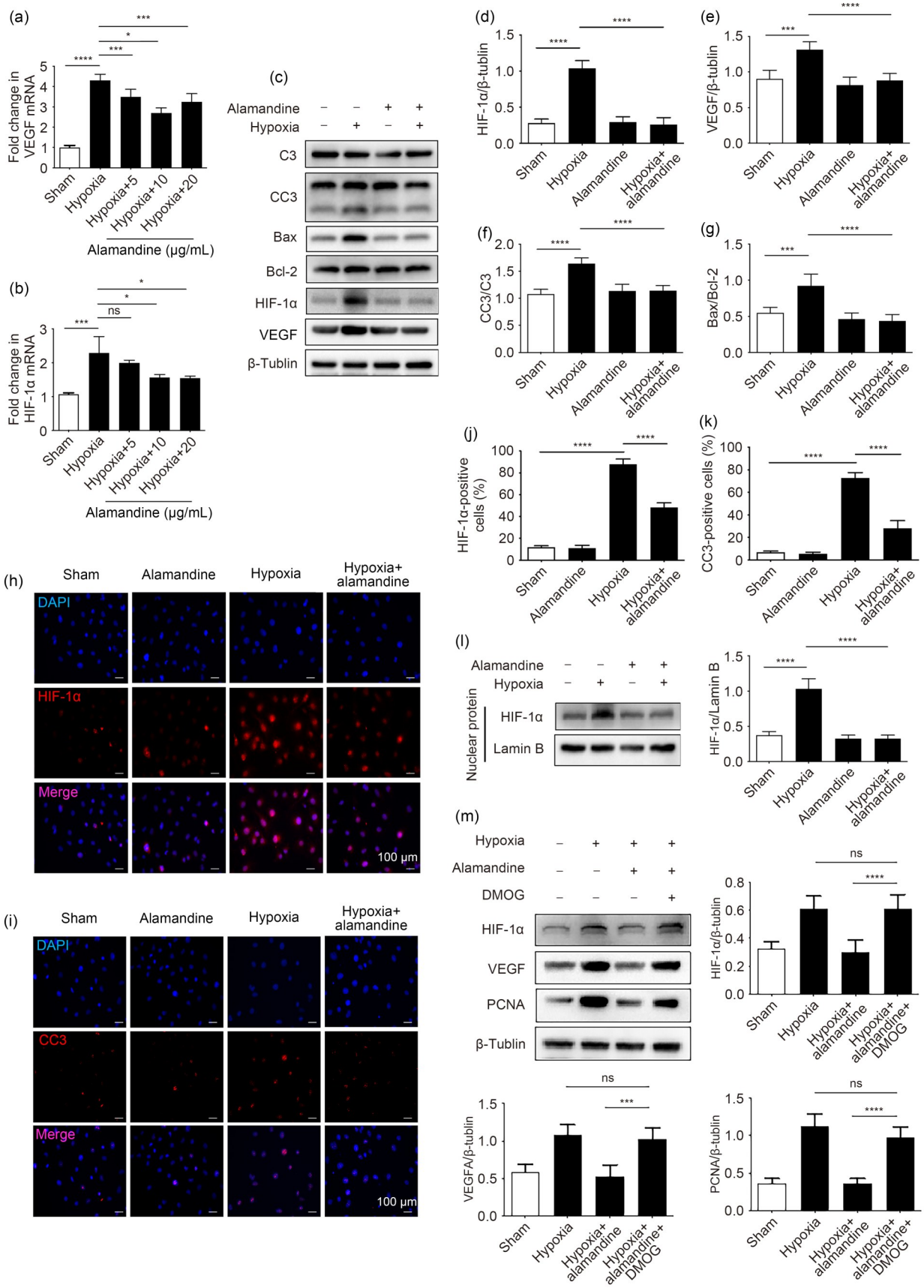
(a)
Fold change in VEGF mRNA
Sham
Hypoxia
Hypoxia+5
Hypoxia+10
Hypoxia+20
Alamandine (μg/mL)
(b)
Fold change in HIF-1α mRNA
(c)
Alamandine
Hypoxia
C3
CC3
Bax
Bcl-2
HIF-1α
VEGF
β-Tublin
(d)
HIF-1α/β-tublin
(e)
VEGF/β-tublin
(f)
CC3/C3
(g)
Bax/Bcl-2
(h)
Sham
Alamandine
Hypoxia
Hypoxia+ alamandine
DAPI
HIF-1α
Merge
100 μm
(i)
CC3
(j)
HIF-1α-positive cells (%)
(k)
CC3-positive cells (%)
(l)
Nuclear protein
Lamin B
HIF-1α/Lamin B
(m)
DMOG
VEGF
PCNA
Hypoxia+ alamandine+ DMOG
VEGFA/β-tublin
PCNA/β-tublin
ns

Fig. 5 Effects of alamandine on hypoxia-induced hypoxia-inducible factor-1α (HIF-1α)/vascular endothelial growth factor (VEGF) pathway activation and apoptosis in human retinal microvascular endothelial cells (HRMECs). (a, b) Messenger RNA (mRNA) expression levels of *VEGF* (a) and *HIF-1α* (b) in HRMECs from different groups determined by the quantitative reserve transcription-polymerase chain reaction (qRT-PCR) method. (c) Protein expression levels of caspase-3 (C3), cleaved caspase-3 (CC3), B cell lymphoma-2 (Bcl-2)-associated X (Bax), Bcl-2, HIF-1α, VEGF, and β-tublin determined by western blot in HRMECs from the sham, hypoxia, alamandine, and hypoxia+alamandine groups. (d–g) Corresponding densitometric analyses of HIF-1α (d), VEGF (e), CC3/C3 (f), and Bax/Bcl-2 (g) protein expression. β-Tublin was detected as the loading control. (h, i) Representative immunofluorescence images of HRMECs labeled with HIF-1α (h) and CC3 (i) from the sham, alamandine, hypoxia, and hypoxia+alamandine groups (HIF-1α: red; CC3: red; 4',6-diamidino-2-phenylindole (DAPI): blue). (j, k) Corresponding quantification of HIF-1α-positive (j) or CC3-positive (k) cells in the chosen images. (l) Nuclear protein expression levels of HIF-1α and Lamin B determined by western blot in HRMECs from the sham, hypoxia, alamandine, and hypoxia+alamandine groups (left) and its corresponding densitometric analysis (right). (m) Protein expression levels of HIF-1α, VEGF, and proliferating cell nuclear antigen (PCNA) were determined by western blot in HRMECs from the sham, hypoxia, hypoxia+alamandine, and hypoxia+alamandine+dimethyloxalylglycine (DMOG) groups, and the corresponding densitometric analysis. All the results are expressed as mean±standard error of mean (SEM) (*n*=5 per group). ns: not significant; * *P*<0.05, *** *P*<0.001, **** *P*<0.0001.

results, the immunofluorescence intensities of HIF-1α- or VEGF-positive cells in mouse retinal paraffin sections from the OIR group were raised compared to those of the control group and were reduced in alamandine-treated OIR mice (Fig. 6j). The above results revealed that alamandine could inhibit vessel proliferation and activation of the HIF-1α/VEGF pathway, thereby attenuating OIR-induced pathological RNV.

3.7 Effects of alamandine on glial cell dysfunction and inflammation in the retinas of OIR mice

The indispensable role of retinal glial cell function has been reported to regulate the integrity of retinal vasculature involved in the pathological retinal angiogenesis of ROP. To determine the effects of alamandine on hypoxia-induced retinal glial cell dysfunction in OIR mouse models, we used immunofluorescence-specific antibodies glial fibrillary acidic protein (GFAP) and ionized calcium-binding adaptor molecule 1 (iba1) to label astrocytes and microglial cells in mouse retinas, respectively. As shown in Fig. 7a, compared with the control group, an OIR-induced drop in astrocyte density was observed in both retinal avascular and neovascular areas. Unlike the uniform distribution of astrocytes in the retinas of the control group, their distribution in the OIR group was destroyed by hypoxic injury. However, alamandine treatment could restore the normal density and distribution of astrocytes in OIR retinas. In addition, the immunofluorescence intensity of activated retinal microglia in the OIR group was increased compared with the control group, which was reduced after the administration of alamandine in OIR-treated mice (Fig. 7b).

Considering that retinal glial cell dysfunction can lead to the excessive production of pro-inflammatory cytokines (Au and Ma, 2022), we investigated the effects of alamandine on the OIR-induced release of pro-inflammatory cytokines. As shown in Fig. 7c, the mRNA expression of interleukin-1β (*IL-1β*), *IL-6*, tumor necrosis factor-α (*TNF-α*), monocyte chemoattractant protein-1 (*MCP-1*), matrix metalloproteinase-9 (*MMP-9*), and cyclooxygenase-2 (*COX-2*), as well as intercellular adhesion molecule-1 (*ICAM-1*) and vascular cell adhesion molecule-1 (*VCAM-1*), was all upregulated in retinal tissues from the OIR group, and alamandine treatment could downregulate OIR-induced elevations of the above pro-inflammatory cytokines. Meanwhile, western blot results showed that the protein expression of oxidative stress-associated iNOS and eNOS was increased in the retinas of the OIR group and was decreased after administration of alamandine (Figs. 7d and 7e). These results indicated that alamandine could improve OIR-induced retinal glial cell dysfunction and inflammation.

3.8 Role of MrgD in the protective effects of alamandine against hypoxia-induced pathological angiogenesis

Alamandine has been reported to exert bioactive effects via its endogenous receptor MrgD (Schleifenbaum, 2019). In our study, alamandine treatment could increase the protein expression of MrgD in HRMECs in a time-dependent manner (Figs. S4a and S4b). Next, we investigated the role of MrgD in the beneficial effects of alamandine on pathological angiogenesis. In vitro, coincubation with D-Pro^{7} (MrgD and Mas receptor antagonist), but not with A779 (specific Mas

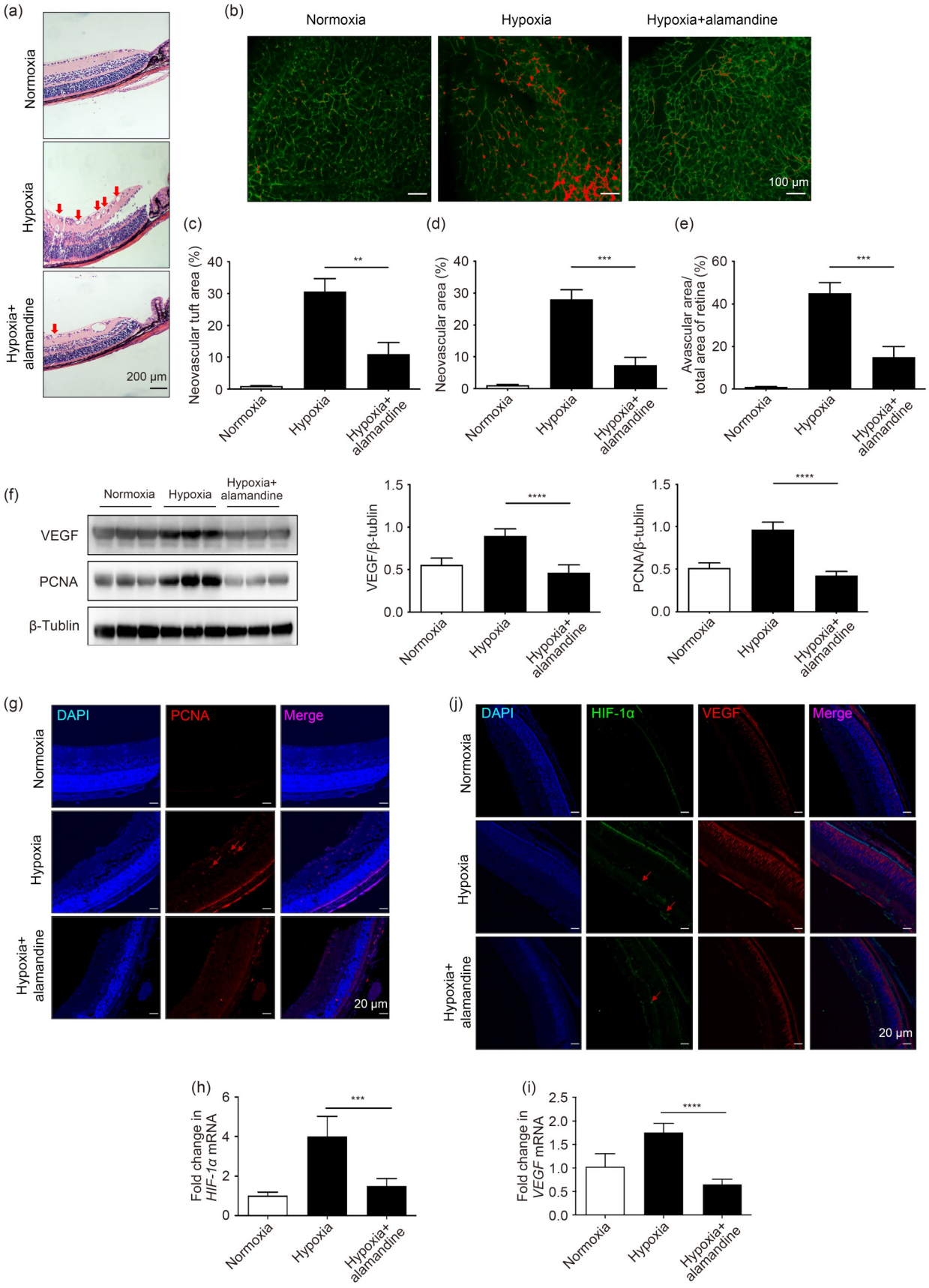
(a)
Normoxia
Hypoxia
Hypoxia+ alamandine
200 μm
(b)
Normoxia
Hypoxia
Hypoxia+alamandine
100 μm
(c)
Neovascular tuft area (%)
(d)
Neovascular area (%)
(e)
Avascular area/ total area of retina (%)
(f)
VEGF
PCNA
β-Tublin
VEGF/β-tublin
PCNA/β-tublin
(g)
DAPI
PCNA
Merge
20 μm
(j)
DAPI
HIF-1α
VEGF
Merge
20 μm
(h)
Fold change in HIF-1α mRNA
(i)
Fold change in VEGF mRNA

Fig. 6 Effects of alamandine on pathological neovascularization in the retinas of oxygen-induced retinopathy (OIR) mice. Mouse retinas were harvested from the normoxia, hypoxia, and hypoxia+alamandine groups. (a) Representative images of retinal paraffin section staining with hematoxylin and eosin (H&E) from the given groups. The arrows indicated neovascular areas. (b) Representative images of retinal whole-mount immunostaining with isolectin B4 (IB4) from the given groups (blood vessels: green; neovascularized areas: red); (c–e) Corresponding quantification of neovascular tuft areas (c), avascular areas (d), and avascular areas/total areas (e). (f) Protein expression levels of vascular endothelial growth factor (VEGF) and proliferating cell nuclear antigen (PCNA) determined by western blot in retinal tissues from the given groups (left) and their corresponding densitometric analysis (right). β-Tublin was detected as the loading control. (g) Representative immunofluorescence images of retinal paraffin sections stained with PCNA and 4',6-diamidino-2-phenylindole (DAPI) from the given groups (PCNA: red; DAPI: blue). (h, i) Messenger RNA (mRNA) expression levels of hypoxia-inducible factor-1α (*HIF-1α*) (h) and *VEGF* (i) in retinal tissues from the given groups determined by the quantitative reserve transcription-polymerase chain reaction (qRT-PCR) method. All mRNA expression was normalized to β-actin. (j) Representative immunofluorescence images of retinal paraffin sections stained with HIF-1α, VEGF, and DAPI from the given groups (HIF-1α: green; VEGF: red; DAPI: blue). The arrow indicates positive staining. All the results are expressed as mean±standard error of mean (SEM) (*n*=6 per group). ** *P*<0.01, *** *P*<0.001, **** *P*<0.0001.

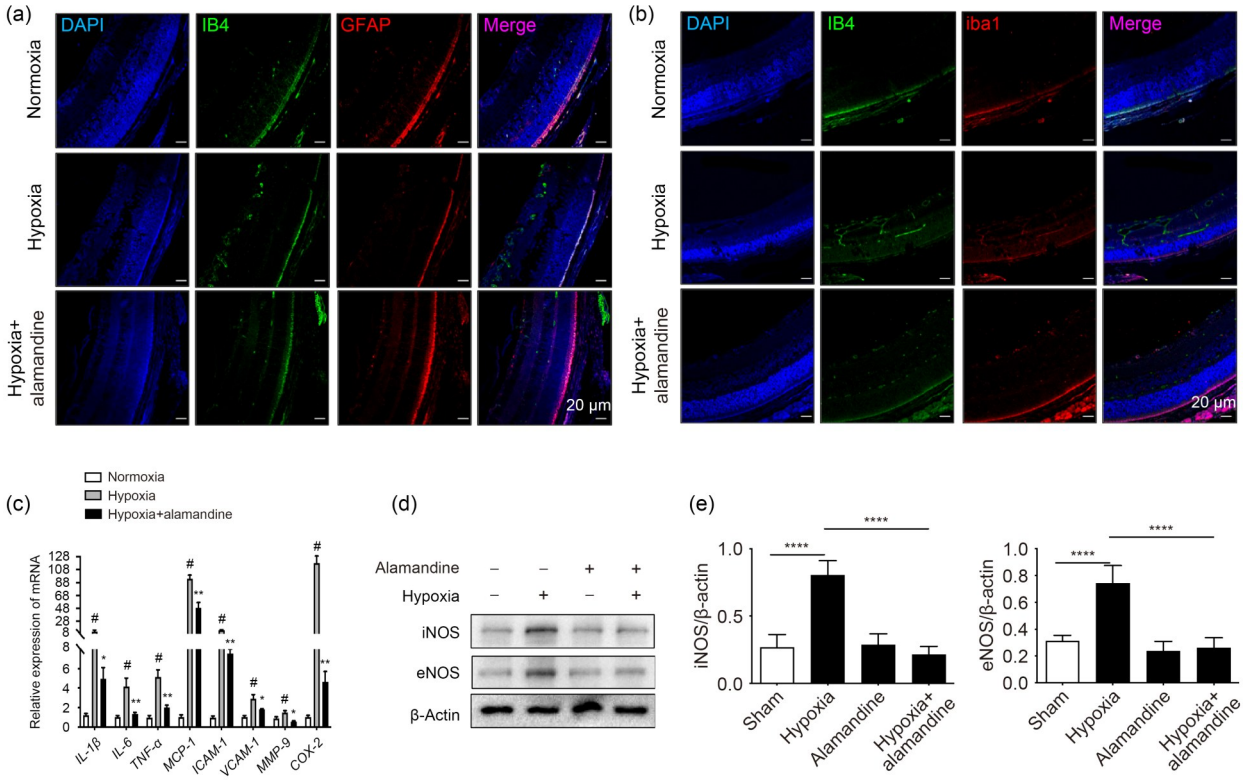

Fig. 7 Effects of alamandine on glial cell dysfunction and inflammation in the retinas of oxygen-induced retinopathy (OIR) mice. Mouse retinas were harvested from the normoxia, hypoxia, and hypoxia+alamandine groups. (a) Representative immunofluorescence images of retinal paraffin sections stained with isolectin B4 (IB4), glial fibrillary acidic protein (GFAP), and 4',6-diamidino-2-phenylindole (DAPI) from the given groups (IB4: green; GFAP: red; DAPI: blue). (b) Representative immunofluorescence images of retinal paraffin sections stained with IB4, ionized calcium-binding adaptor molecule 1 (iba1), and DAPI from the given groups (IB4: green; iba1: red; DAPI: blue). (c) Messenger RNA (mRNA) expression levels of interleukin-1β (*IL-1β*), *IL-6*, tumor necrosis factor-α (*TNF-α*), monocyte chemoattractant protein-1 (*MCP-1*), matrix metalloproteinase-9 (*MMP-9*), and cyclooxygenase-2 (*COX-2*), as well as intercellular adhesion molecule-1 (*ICAM-1*) and vascular cell adhesion molecule-1 (*VCAM-1*) in retinal tissues from the given groups determined by quantitative reserve transcription-polymerase chain reaction (qRT-PCR) method. All mRNA expression was normalized to β-actin. * *P*<0.05, ** *P*<0.01 vs. hypoxia group; $^{\#}$ *P*<0.05 vs. normoxia group. (d) Protein expression levels of inducible nitric oxide synthase (iNOS) and endothelial nitric oxide synthase (eNOS) determined by western blot in retinal tissues from the given groups. β-Actin was detected as the loading control. All the results are expressed as mean±standard error of mean (SEM) (*n*=5 per group). **** *P*<0.0001.

receptor antagonist) or PD123319 (AT2 receptor (AT_2R) inhibitor), could block the downregulation of HIF-1α and VEGF induced by alamandine in hypoxia-treated HRMECs (Figs. S4c and S4d). In vivo, mouse models were pre-treated with D-Pro^7, PD123319, or A779 in the presence of hypoxia and alamandine. As shown in Figs. 8a–8d, pre-treatment with D-Pro^7 could reverse the protective effects of alamandine against OIR-induced retinal avascular zones and neovascularization tufts, while A779 failed. Corroborating this finding, the same trend was also found in the protein expression of HIF-1α and VEGF (Fig. 8e). Accordingly, we could infer that alamandine did play an anti-angiogenesis role through the HIF-1α/VEGF

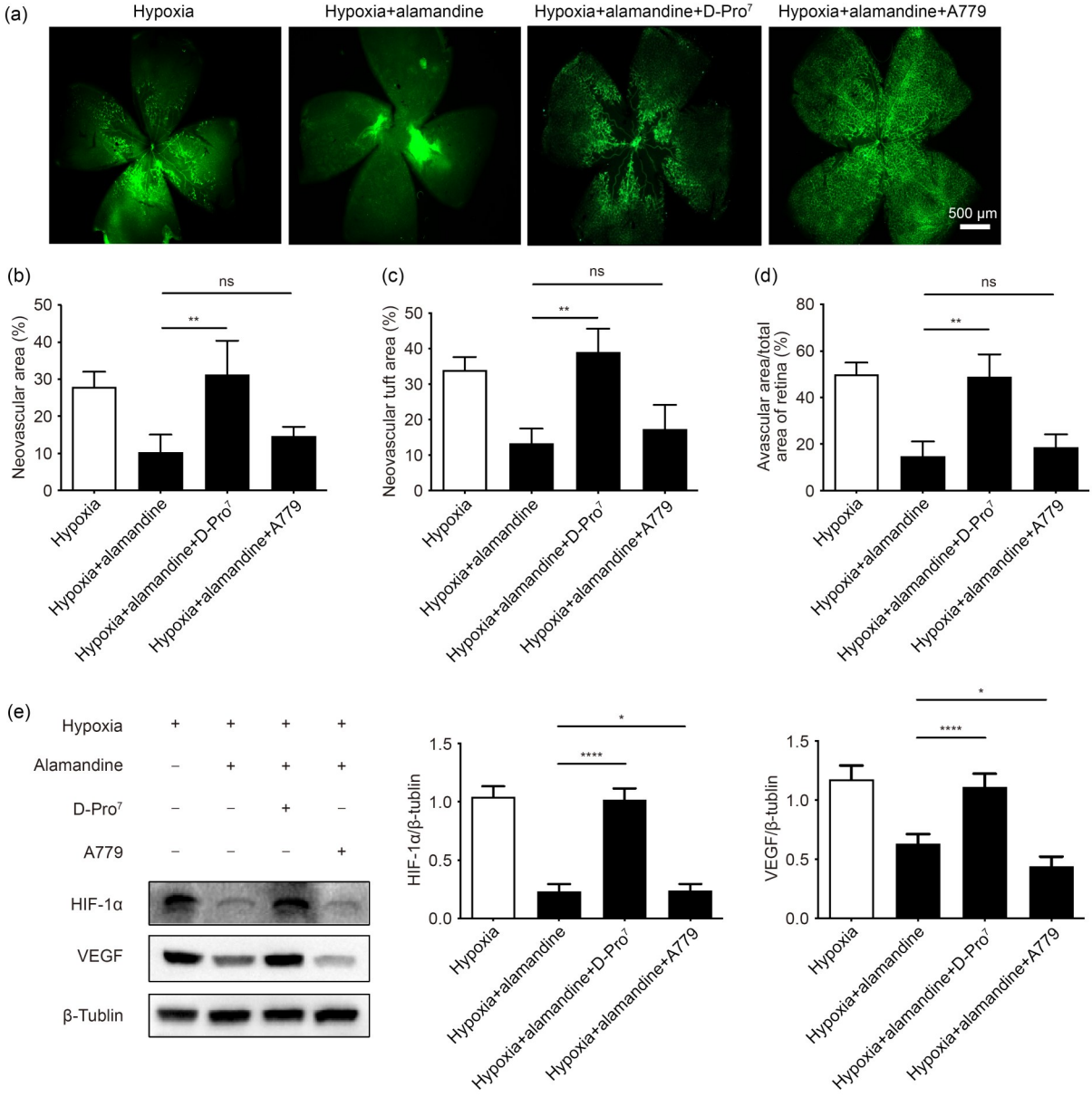

Fig. 8 Role of Mas-related G protein-coupled receptor D (MrgD) in the protective effects of alamandine against hypoxia-induced pathological angiogenesis in mice. (a) Representative images of retinal whole-mount immunostaining with isolectin B4 (IB4) from the different groups. (b–d) Corresponding quantification of avascular areas (b), neovascular tuft areas (c), and avascular areas/total areas (d). (e) Protein expression levels of hypoxia-inducible factor-1α (HIF-1α) and vascular endothelial growth factor (VEGF) determined by western blot in mice retinas from the different groups (left) and the corresponding densitometric analysis (right). β-Tublin was detected as the loading control. All the results are expressed as mean±standard error of mean (SEM) (n=6 per group). ns: not significant; * P<0.05, ** P<0.01, **** P<0.0001.

pathway via MrgD in hypoxia-induced pathological angiogenesis.

3.9 Role of MrgD in the protective effects of alamandine against glial cell dysfunction and inflammation in the retinas of OIR mice

We next investigated the participation of the MrgD receptor in alamandine's effects on OIR-induced retinal glial cell dysfunction and inflammation. As shown in Fig. S5a, D-Pro^7 pre-treatment could counteract the action of alamandine in down-regulating OIR-induced mRNA expression of various pro-inflammatory cytokines, including *IL-1β*, *IL-6*, *TNF-α*, *MCP-1*, *COX-2*, and *MMP-9*, as well as *ICAM-1* and *VCAM-1* in the retinas. Also, the protective effects of alamandine on restoring the normal density and distribution of retinal astrocytes and microglial cells in the OIR-treated mouse were inhibited by D-Pro^7 pre-treatment (Figs. S5b and S5c). Taken together, the above studies indicated that alamandine could improve OIR-induced retinal glial cell dysfunction and inflammation, thus attenuating pathological angiogenesis by regulating the HIF-1α/VEGF pathway via MrgD.

4 Discussion

To our knowledge, this work proved for the first time that alamandine has a protective role in improving hypoxia-induced retinal microvascular dysfunction and pathological neovascularization by inhibiting the activation of the HIF-1α/VEGF pathway via MrgD in OIR mice.

Considering the similar pathogenesis and pathological features, the tested mouse models of OIR have been widely used to resemble ROP for their convenience in terms of observation, which allows us to explore the potential molecular mechanisms (Rivera et al., 2016). ROP (initially termed retrolental fibroplasia) is an ischemia-induced proliferative retinal vasculopathy that occurs in premature infants, ultimately causing vision impairment and even blindness (Daruich et al., 2020). As ROP progresses, various hypoxia-induced pathological changes, including but not limited to blood–retinal barrier (BRB) damage, vascular hyperpermeability, and inflammation, have been identified to facilitate the formation of intravitreal neovascular tufts through activating HIF-1α-dependent VEGF activity and other signaling pathways (Broxterman and Hug, 2016; Guo et al., 2020).

Various cell types, which consisted of retina, exerted their distinct effects under retinal pathological conditions (Voigt et al., 2021), which remained to be fully elucidated. Emerging evidence from scRNA-seq studies has revolutionized our understanding of heterogeneity of ECs and their functional contributions to RNV progression (Cheng et al., 2024; He et al., 2024), thereby providing critical insights for therapeutic targeting. The integration of multi-species scRNA-seq data in our study represented a paradigm shift in retinal vascular biology research, significantly enhancing both the scientific rigor and translational relevance of our study on RNV. Here, we also found that ECs were highly related to RNV via scRNA-seq data analysis. Besides, the cell-type-specific signatures identified through scRNA-seq could guide the development of precision therapies (Au and Ma, 2022; Zhang et al., 2024). For instance, EC clusters with high angiogenic factor with G-patch and forkhead-associated domain 1 (AGGF1) expression were related to advanced RNV stages (Cheng et al., 2025). In our study, we found that RAS-associated ECs may respond to RNV as well.

RAS played a pivotal role in regulating EC function during various diseases (Moravski et al., 2003; Amraei and Rahimi, 2020). Multiple biological compounds involved in the RAS are widely expressed in the retina (Paul et al., 2006). Notably, genetically engineered mice have elucidated the causal role of RAS in retinal pathological neovascularization. For example, a previous study has revealed that EC-specific deletion of adenosine A2a receptor ($A_{2a}R$) improved OIR-induced retinal angiogenesis in mice (Santiago et al., 2020). RAS-targeted therapies, including small-molecule inhibitors, could suppress hypoxia-driven angiogenesis, underscoring its pathological role (Boddu et al., 2023). Changes in the expression levels of serum RAS members, including Ang-1 and Ang-2, may be promising biomarkers for reflecting the regression and treatment of ROP (Yang et al., 2021; Wang et al., 2023). Among them, serum Ang-(1–7) levels have also been demonstrated to predict the development of retinopathy in diabetics (Duan et al., 2018). Ang-(1–7) has been reported to exert anti-angiogenic and anti-apoptosis effects by inhibiting VEGF activation and HIF-1α nuclear translocation, respectively (de Carvalho Santuchi et al., 2019). It can also play a beneficial role

in cardiovascular diseases by interacting with MrgD, which is a natural endogenous receptor of alamandine. Notably, the expression of MrgD has recently been reported to play a crucial role in retinal neurovascular function (Zhu et al., 2020). As the novel members are involved in the counter-regulatory mechanism within the RAS, the similar molecular structures and receptors between alamandine and Ang-(1–7) may account for their similar protective actions (Schleifenbaum, 2019). Thus, we used the LC-MS/MS method to explore the possible changes in alamandine and some other RAS members related to the generation of alamandine in the retina and serum, and further investigated a new possible mechanism in the treatment of ROP. In our initial studies, lower expression levels of alamandine and higher levels of Ang II in serum and retinas were found in ROP infants compared with their age-matched healthy subjects through the LC-MS/MS method. Thus, further investigations were undertaken to examine whether alamandine could inhibit OIR-induced angiogenesis. Our data showed that alamandine could attenuate VEGF- or hypoxia-induced HRMEC proliferation, microvascular sprouting, and migration, meaning that it can reduce pathological angiogenesis in neovascular areas. Moreover, alamandine improved hypoxia-induced RNV and vascular dysfunction in mouse models of OIR dose-dependently.

In the process of vascular invasion involved in the formation of neovessels with functional defects and structural abnormalities, the endoproteases MMPs have been reported to play a critical role in vitreous leakage and hemorrhage (Choręziak-Michalak et al., 2023). In our study, in agreement with the presence of increased MMP expression reported in the vitreous of ROP patients (Rathi et al., 2017), elevated levels of MMP-9 after hypoxia stimulation were found in vivo and in vitro, which can be decreased by alamandine treatment.

Retinal hemorrhage found in ROP indicates the presence of a disrupted and hyperpermeable vascular barrier system consisting of retinal glial cells (Hartnett, 2023). Regarding the reported indispensable and mutually reinforcing relationships between pathologic retinal angiogenesis and retinal glial dysfunction during pathological development in mouse models of OIR, since alamandine could attenuate hypoxia-induced neovascularization, it may be able to restore the integrity of retinal vasculature (Karlstetter et al., 2015). As the variants of macroglia, both astrocytes and Miiller cells are involved in the normal development of the retinal vessels by wrapping around retinal ganglion cells' axon bundles that are essential for the formation of the BRB (Li et al., 2019). It has been established that the hypoxia-induced distribution of retinal astrocytes located within the nerve fiber layer from the optic disc into vascularized retinas could result in the disorderly formation of neovascular tufts in the avascular area of ROP (Perelli et al., 2021). Additionally, the oxygen-induced injury may induce astrocytes to secret VEGF, contributing to pathological neovascularization (Rathi et al., 2017). GFAP-like immunoreactivity is well-recognized to label astrocytes in the retina, making it viable for further studies (Brenner and Messing, 2021). In our study, alamandine treatment could significantly reduce newly induced vessels and vascular leakage in the remodeling retinal zone of OIR by restoring the normal density and distribution of astrocytes.

In the case of oxygen-induced injury, activated microglia cells have also been evidenced to cluster around retinal neovessels in a disorderly manner and produce excessive pro-inflammatory cytokines, including TNF-α, IL-1β, IL-6, and MCP-1, thus promoting the pathological progression of OIR in mouse models (Checchin et al., 2006; Aouiss et al., 2019). Then, the increased inflammation may contribute to the potentiated oxidative stress, resulting in the uncoupling of eNOS and the decreased release of nitric oxide (NO) derived from eNOS in the vasculature (Li et al., 2014). Similar to Ang-(1–7), alamandine has also been demonstrated to have anti-inflammatory and anti-proliferation effects on cardiovascular diseases by regulating the pro-inflammatory signaling cascade, and NO production responded to pathological stimulus in cardiomyocytes and endothelial cells via interacting with the MrgD receptor (de Jesus et al., 2018; Zhao et al., 2022a). In our study, alamandine treatment could inhibit the migration and activation of microglia cells, accompanied by the reduced production of pro-inflammatory cytokines in the OIR. These data could also support the notion that alamandine inhibits OIR-induced microvascular injury and pathological angiogenesis by suppressing inflammation and oxidative stress.

In response to hypoxia-activated oxidative stress and immune response in endothelial cells, multiple related signaling pathways are activated, among which the HIF-1α/VEGF pathway has been suggested as

the most crucial (Zhao et al., 2023). It has been reported that hypoxia-induced HIF-1α/dependent VEGF stimulation is most closely related to hypoxia-induced RNV in ROP (Dong et al., 2021; Zhao et al., 2022b). Under hypoxic or anaerobic conditions, HIF-1α becomes stable. After being translocated into the nucleus, accumulated HIF-1α dimerizes with the HIF-1β subunit, which is essential for the emergence of endothelial cells during the embryonic period (Rattner et al., 2019). Then, the HIF-1α/β dimer promotes vasculogenesis by activating the transcriptional activity of the proangiogenic genes like *VEGF* (Vallée et al., 2018). VEGF, the most important factor that favors vast proliferation and angiogenesis, is secreted by hypoxia-induced microglial cells, leading to abnormal neovascularization in mouse models of OIR (Lashkari et al., 2000; Rathi et al., 2017). In our study, alamandine treatment could reduce hypoxia-induced nuclear import of HIF-1α, as well as the expression of HIF-1α and VEGF in HRMECs, suggesting that alamandine exerts its protective effects against ROP through inactivating the HIF-1α/VEGF pathway.

MrgD, also called TGR7, is one of the members of the G protein-coupled receptor (GPCR) family that plays a crucial role in regulating inflammation and vascular endothelium function involved in the pathophysiological development of cardiovascular remodeling (de Jesus et al., 2023). Several previous studies have reported that alamandine could elicit its bioactive effects in the cardiovascular system by activating the MrgD receptor (Lautner et al., 2013; Schleifenbaum, 2019; Zhao et al., 2023). Interestingly, alamandine treatment was demonstrated to improve vascular fibrosis via upregulating MrgD expression (Yang et al., 2020). Additionally, we previously reported that alamandine alone could stimulate MrgD expression in primary neonatal rat cardiomyocytes (NRCMs) and primary neonatal rat cardiac fibroblasts (NRCFs) (Zhao et al., 2023). More importantly, while losartan upregulated the levels of its receptor angiotensin II type 1 (AT1) receptor (AT_1R) in the left ventricle in a negative feedback manner (Song et al., 2015), alamandine was deemed an MrgD blocker that elevated MrgD expression in a negative feedback manner (Zhao et al., 2023). In our study, we found that alamandine treatment upregulated MrgD expression in vivo and in vitro.

Since the alamandine/MrgD axis has been considered a novel protective mechanism against retinal diseases (Zhu et al., 2020), we speculated that alamandine may inhibit hypoxia-induced pathological angiogenesis via MrgD. As an AT_2R inhibitor, PD123319 is also regarded as an MrgD receptor antagonist, which can attenuate the protective effects of alamandine or Ang-(1–7) in some studies, but not all (Park et al., 2018). Additionally, D-Pro^7 can block the binding of alamandine to the MrgD receptor and the Mas receptor through competitive inhibition. It has been evidenced that the cardioprotective actions of alamandine can be blocked by pre-treatment with D-Pro^7 (Park et al., 2018). In our study, the beneficial role of alamandine in inhibiting hypoxia-induced activation of the HIF-1α/VEGF pathway was reversed after coincubation with D-Pro^7 but not with PD123319. However, the inhibitory effects of alamandine on mitogen-activated protein kinase (MAPK) and phosphatidylinositol 3-kinase/protein kinase B/mechanistic target of rapamycin (PI3K/AKT/mTOR) signaling pathways were not blocked. Furthermore, the protective effects of alamandine on improving hypoxia- or VEGF-induced HRMEC proliferation, microvascular sprouting, and migration were not abolished by pre-treatment with the specific Mas receptor antagonist, A779, suggesting that alamandine did exert its anti-angiogenesis effects by regulating the HIF-1α/VEGF pathway via MrgD.

5 Conclusions

Taken together, this work integrally demonstrated that alamandine could improve hypoxia-induced retinal vascular barrier dysfunction with a restored glial cell network and alleviate inflammation response. Thus, alamandine inhibits retinal pathological neovascularization by inhibiting the HIF-1α/VEGF pathway via MrgD in OIR mouse models, paving the way for future clinical application of alamandine in ROP.

Data availability statement

All data supporting the findings of this study are available within the paper and its supplementary information.

Acknowledgments

This work was supported by the National Natural Science Foundation of China (Nos. 82200379 and 82300309), the Shanghai Sailing Program (No. 22YF1443100), the Academy Talent Special Fund of The First Affiliated Hospital of Nanjing

Medical University (Nos. YNRCQN0312 and MXJL202208), and the Jiangsu Funding Program for Excellent Postdoctoral Talent (No. 2023ZB592), China.

Author contributions

Kun ZHAO conceived the study, coordinated the scientific team, and allocated the funding for the project; Yaping JIANG performed the experimental research and data analysis; Wen HUANG performed the establishment of animal models; Yukang MAO wrote and edited the manuscript; Yihui CHEN conceived the study; Peng LI coordinated the scientific team and reviewed the manuscript; Chuanxi YANG conceived the study, coordinated the scientific team, and allocated the funding for the project. All authors have read and approved the final manuscript, and therefore, have full access to all the data in the study and take responsibility for the integrity and security of the data.

Compliance with ethics guidelines

Kun ZHAO, Yaping JIANG, Wen HUANG, Yukang MAO, Yihui CHEN, Peng LI, and Chuanxi YANG declare that they have no conflicts of interest.

The experimental protocols have gained approval from the Experimental Animal Care and Use Committee of Nanjing Medical University, and were implemented in compliance with the Guidelines on the Care and Use of Laboratory Animals (the National Institute of Health (NIH) publication No. 85-23, revised 1996).

References

Ahmed NEMB, Murakami M, Kaneko S, et al., 2016. The effects of hypoxia on the stemness properties of human dental pulp stem cells (DPSCs). *Sci Rep*, 6:35476. https://doi.org/10.1038/srep35476

Amraei R, Rahimi N, 2020. COVID-19, renin-angiotensin system and endothelial dysfunction. *Cells*, 9(7):1652. https://doi.org/10.3390/cells9071652

Aouiss A, Anka Idrissi D, Kabine M, et al., 2019. Update of inflammatory proliferative retinopathy: ischemia, hypoxia and angiogenesis. *Curr Res Transl Med*, 67(2):62-71. https://doi.org/10.1016/j.retram.2019.01.005

Au NPB, Ma CHE, 2022. Neuroinflammation, microglia and implications for retinal ganglion cell survival and axon regeneration in traumatic optic neuropathy. *Front Immunol*, 13:860070. https://doi.org/10.3389/fimmu.2022.860070

Boddu SHS, Acharya D, Hala V, et al., 2023. An update on strategies to deliver protein and peptide drugs to the eye. *ACS Omega*, 8(39):35470-35498. https://doi.org/10.1021/acsomega.3c02897

Brenner M, Messing A, 2021. Regulation of GFAP expression. *ASN Neuro*, 13:1759091420981206. https://doi.org/10.1177/1759091420981206

Broxterman EC, Hug DA, 2016. Retinopathy of prematurity: a review of current screening guidelines and treatment options. *Mo Med*, 113(3):187-190.

Chang E, Josan AS, Purohit R, et al., 2022. A network meta-analysis of retreatment rates following bevacizumab, ranibizumab, aflibercept, and laser for retinopathy of prematurity. *Ophthalmology*, 129(12):1389-1401. https://doi.org/10.1016/j.ophtha.2022.06.042

Chang RL, Lin JW, Kuo WW, et al., 2016. Angiotensin-(1–7) attenuated long-term hypoxia-stimulated cardiomyocyte apoptosis by inhibiting HIF-1α nuclear translocation via Mas receptor regulation. *Growth Factors*, 34(1-2):11-18. https://doi.org/10.3109/08977194.2016.1155150

Checchin D, Sennlaub F, Levavasseur E, et al., 2006. Potential role of microglia in retinal blood vessel formation. *Invest Ophthalmol Vis Sci*, 47(8):3595-3602. https://doi.org/10.1167/iovs.05-1522

Cheng Y, Zhang M, Xu R, et al., 2024. P53 accelerates endothelial cell senescence in diabetic retinopathy by enhancing FoxO3a ubiquitylation and degradation via UBE2L6. *Exp Gerontol*, 188:112391. https://doi.org/10.1016/j.exger.2024.112391

Cheng Y, Zhang M, Li CG, et al., 2025. Endothelial AGGF1 promotes retinal angiogenesis by coordinating TNFSF12/FN14 signalling. *Nat Commun*, 16:1332. https://doi.org/10.1038/s41467-025-55970-3

Choręziak-Michalak A, Szpecht D, Chmielarz-Czarnocińska A, et al., 2023. Comprehensive analysis of the role of gene variants in matrix metalloproteinases and their tissue inhibitors in retinopathy of prematurity: a study in the Polish population. *Int J Mol Sci*, 24(20):15309. https://doi.org/10.3390/ijms242015309

Connor KM, Krah NM, Dennison RJ, et al., 2009. Quantification of oxygen-induced retinopathy in the mouse: a model of vessel loss, vessel regrowth and pathological angiogenesis. *Nat Protoc*, 4(11):1565-1573. https://doi.org/10.1038/nprot.2009.187

Dammann O, Hartnett ME, Stahl A, 2023. Retinopathy of prematurity. *Dev Med Child Neurol*, 65(5):625-631. https://doi.org/10.1111/dmcn.15468

Daruich A, Bremond-Gignac D, Behar-Cohen F, et al., 2020. Retinopathy of prematurity: from prevention to treatment. *Med Sci (Paris)*, 36(10):900-907. https://doi.org/10.1051/medsci/2020163

de Carvalho Santuchi M, Dutra MF, Vago JP, et al., 2019. Angiotensin-(1–7) and alamandine promote anti-inflammatory response in macrophages *in vitro* and *in vivo*. *Mediators Inflamm*, 2019:2401081. https://doi.org/10.1155/2019/2401081

de Jesus ICG, Scalzo S, Alves F, et al., 2018. Alamandine acts via MrgD to induce AMPK/NO activation against Ang II hypertrophy in cardiomyocytes. *Am J Physiol Cell Physiol*, 314(6):C702-C711. https://doi.org/10.1152/ajpcell.00153.2017

de Jesus ICG, Mesquita T, Souza Santos RA, et al., 2023. An overview of alamadine/MrgD signaling and its role in cardiomyocytes. *Am J Physiol Cell Physiol*, 324(3):C606-C613. https://doi.org/10.1152/ajpcell.00399.2021

Domińska K, Okła P, Kowalska K, et al., 2018. Angiotensin 1–7 modulates molecular and cellular processes central to the pathogenesis of prostate cancer. *Sci Rep*, 8:15772. https://doi.org/10.1038/s41598-018-34049-8

Dong LJ, Li WB, Lin TT, et al., 2021. PSF functions as a repressor of hypoxia-induced angiogenesis by promoting mitochondrial function. *Cell Commun Signal*, 19:14. https://doi.org/10.1186/s12964-020-00684-w

Duan YQ, Beli E, Li Calzi S, et al., 2018. Loss of angiotensin-converting enzyme 2 exacerbates diabetic retinopathy by promoting bone marrow dysfunction. *Stem Cells*, 36(9): 1430-1440. https://doi.org/10.1002/stem.2848

Fevereiro-Martins M, Marques-Neves C, Guimarães H, et al., 2023. Retinopathy of prematurity: a review of pathophysiology and signaling pathways. *Surv Ophthalmol*, 68(2): 175-210. https://doi.org/10.1016/j.survophthal.2022.11.007

Guo Y, Gu RP, Gan DK, et al., 2020. Mitochondrial DNA drives noncanonical inflammation activation via cGAS-STING signaling pathway in retinal microvascular endothelial cells. *Cell Commun Signal*, 18:172. https://doi.org/10.1186/s12964-020-00637-3

Hartnett ME, 2023. Pathophysiology of retinopathy of prematurity. *Annu Rev Vis Sci*, 9:39-70. https://doi.org/10.1146/annurev-vision-093022-021420

He XM, Wen SY, Tang XX, et al., 2024. Glucagon-like peptide-1 receptor agonists rescued diabetic vascular endothelial damage through suppression of aberrant STING signaling. *Acta Pharm Sin B*, 14(6):2613-2630. https://doi.org/10.1016/j.apsb.2024.03.011

Hu ZZ, Mao XY, Chen MK, et al., 2022. Single-cell transcriptomics reveals novel role of microglia in fibrovascular membrane of proliferative diabetic retinopathy. *Diabetes*, 71(4):762-773. https://doi.org/10.2337/db21-0551

Huang H, 2020. Pericyte-endothelial interactions in the retinal microvasculature. *Int J Mol Sci*, 21(19):7413. https://doi.org/10.3390/ijms21197413

Karlstetter M, Scholz R, Rutar M, et al., 2015. Retinal microglia: just bystander or target for therapy? *Prog Retin Eye Res*, 45:30-57. https://doi.org/10.1016/j.preteyeres.2014.11.004

Lashkari K, Hirose T, Yazdany J, et al., 2000. Vascular endothelial growth factor and hepatocyte growth factor levels are differentially elevated in patients with advanced retinopathy of prematurity. *Am J Pathol*, 156(4):1337-1344. https://doi.org/10.1016/s0002-9440(10)65004-3

Lautner RQ, Villela DC, Fraga-Silva RA, et al., 2013. Discovery and characterization of alamandine: a novel component of the renin–angiotensin system. *Circ Res*, 112(8): 1104-1111. https://doi.org/10.1161/circresaha.113.301077

Li HG, Horke S, Förstermann U, 2014. Vascular oxidative stress, nitric oxide and atherosclerosis. *Atherosclerosis*, 237(1):208-219. https://doi.org/10.1016/j.atherosclerosis.2014.09.001

Li N, Gao S, Wang J, et al., 2019. Anti-apoptotic effect of interleukin-17 in a mouse model of oxygen-induced retinopathy. *Exp Eye Res*, 187:107743. https://doi.org/10.1016/j.exer.2019.107743

Li P, Chen XR, Xu F, et al., 2018. Alamandine attenuates sepsis-associated cardiac dysfunction via inhibiting MAPKs signaling pathways. *Life Sci*, 206:106-116. https://doi.org/10.1016/j.lfs.2018.04.010

Mintz-Hittner HA, Kennedy KA, Chuang AZ, 2011. Efficacy of intravitreal bevacizumab for stage 3+ retinopathy of prematurity. *N Engl J Med*, 364(7):603-615. https://doi.org/10.1056/NEJMoa1007374

Moravski CJ, Skinner SL, Stubbs AJ, et al., 2003. The renin-angiotensin system influences ocular endothelial cell proliferation in diabetes: transgenic and interventional studies. *Am J Pathol*, 162(1):151-160. https://doi.org/10.1016/s0002-9440(10)63806-0

Nicosia RF, Ottinetti A, 1990. Growth of microvessels in serum-free matrix culture of rat aorta. A quantitative assay of angiogenesis in vitro. *Lab Invest*, 63(1):115-122.

Park BM, Phuong HTA, Yu LM, et al., 2018. Alamandine protects the heart against reperfusion injury via the MrgD receptor. *Circ J*, 82(10):2584-2593. https://doi.org/10.1253/circj.CJ-17-1381

Paul M, Poyan Mehr A, Kreutz R, 2006. Physiology of local renin-angiotensin systems. *Physiol Rev*, 86(3):747-803. https://doi.org/10.1152/physrev.00036.2005

Perelli RM, O'Sullivan ML, Zarnick S, et al., 2021. Environmental oxygen regulates astrocyte proliferation to guide angiogenesis during retinal development. *Development*, 148(9):dev199418. https://doi.org/10.1242/dev.199418

Phipps JA, Dixon MA, Jobling AI, et al., 2019. The renin-angiotensin system and the retinal neurovascular unit: a role in vascular regulation and disease. *Exp Eye Res*, 187:107753. https://doi.org/10.1016/j.exer.2019.107753

Rathi S, Jalali S, Patnaik S, et al., 2017. Abnormal complement activation and inflammation in the pathogenesis of retinopathy of prematurity. *Front Immunol*, 8:1868. https://doi.org/10.3389/fimmu.2017.01868

Rattner A, Williams J, Nathans J, 2019. Roles of HIFs and VEGF in angiogenesis in the retina and brain. *J Clin Invest*, 129(9):3807-3820. https://doi.org/10.1172/jci126655

Rivera JC, Madaan A, Zhou TE, et al., 2016. Review of the mechanisms and therapeutic avenues for retinal and choroidal vascular dysfunctions in retinopathy of prematurity. *Acta Paediatr*, 105(12):1421-1433. https://doi.org/10.1111/apa.13586

Sabri K, Ells AL, Lee EY, et al., 2022. Retinopathy of prematurity: a global perspective and recent developments. *Pediatrics*, 150(3):e2021053924. https://doi.org/10.1542/peds.2021-053924

Santiago AR, Madeira MH, Boia R, et al., 2020. Keep an eye on adenosine: its role in retinal inflammation. *Pharmacol Ther*, 210:107513. https://doi.org/10.1016/j.pharmthera.2020.107513

Schleifenbaum J, 2019. Alamandine and its receptor MrgD pair up to join the protective arm of the renin-angiotensin system. *Front Med (Lausanne)*, 6:107. https://doi.org/10.3389/fmed.2019.00107

Song MA, Dasgupta C, Zhang LB, 2015. Chronic losartan treatment up-regulates AT_1R and increases the heart vulnerability to acute onset of ischemia and reperfusion injury in male rats. *PLoS ONE*, 10(7):e0132712. https://doi.org/10.1371/journal.pone.0132712

Tual-Chalot S, Allinson KR, Fruttiger M, et al., 2013. Whole mount immunofluorescent staining of the neonatal mouse

retina to investigate angiogenesis *in vivo*. *J Vis Exp*, (77): e50546.
https://doi.org/10.3791/50546

Uemura A, Fruttiger M, D'Amore PA, et al., 2021. VEGFR1 signaling in retinal angiogenesis and microinflammation. *Prog Retin Eye Res*, 84:100954.
https://doi.org/10.1016/j.preteyeres.2021.100954

Vallée A, Guillevin R, Vallée JN, 2018. Vasculogenesis and angiogenesis initiation under normoxic conditions through Wnt/β-catenin pathway in gliomas. *Rev Neurosci*, 29(1): 71-91.
https://doi.org/10.1515/revneuro-2017-0032

Voigt AP, Mullin NK, Stone EM, et al., 2021. Single-cell RNA sequencing in vision research: insights into human retinal health and disease. *Prog Retin Eye Res*, 83:100934.
https://doi.org/10.1016/j.preteyeres.2020.100934

Wang YH, Fang JW, Niu T, et al., 2023. Serum Ang-1/Ang-2 ratio may be a promising biomarker for evaluating severity of diabetic retinopathy. *Graefes Arch Clin Exp Ophthalmol*, 261(1):49-55.
https://doi.org/10.1007/s00417-022-05745-z

Xu Y, Lu X, Hu YG, et al., 2018. Melatonin attenuated retinal neovascularization and neuroglial dysfunction by inhibition of HIF-1α-VEGF pathway in oxygen-induced retinopathy mice. *J Pineal Res*, 64(4):e12473.
https://doi.org/10.1111/jpi.12473

Yang CX, Wu XG, Shen YH, et al., 2020. Alamandine attenuates angiotensin II-induced vascular fibrosis via inhibiting p38 MAPK pathway. *Eur J Pharmacol*, 883:173384.
https://doi.org/10.1016/j.ejphar.2020.173384

Yang XF, Wang JP, Chen C, 2021. Serum VEGF and Ang-2 levels in infants before and after laser treatment for retinopathy of prematurity. *Fetal Pediatr Pathol*, 40(5): 407-413.
https://doi.org/10.1080/15513815.2020.1721625

Zhang XZ, Zhang F, Xu X, 2024. Single-cell RNA sequencing in exploring the pathogenesis of diabetic retinopathy. *Clin Transl Med*, 14(7):e1751.
https://doi.org/10.1002/ctm2.1751

Zhao K, Xu TH, Mao YK, et al., 2022a. Alamandine alleviated heart failure and fibrosis in myocardial infarction mice. *Biol Direct*, 17:25.
https://doi.org/10.1186/s13062-022-00338-6

Zhao K, Jiang YP, Zhang J, et al., 2022b. Celastrol inhibits pathologic neovascularization in oxygen-induced retinopathy by targeting the miR-17-5p/HIF-1α/VEGF pathway. *Cell Cycle*, 21(19):2091-2108.
https://doi.org/10.1080/15384101.2022.2087277

Zhao K, Hua DX, Yang CX, et al., 2023. Nuclear import of Mas-related G protein-coupled receptor member D induces pathological cardiac remodeling. *Cell Commun Signal*, 21:181.
https://doi.org/10.1186/s12964-023-01168-3

Zhu P, Verma A, Prasad T, et al., 2020. Expression and function of Mas-related G protein-coupled receptor D and its ligand alamandine in retina. *Mol Neurobiol*, 57(1):513-527.
https://doi.org/10.1007/s12035-019-01716-4

Zimna A, Kurpisz M, 2015. Hypoxia-inducible factor-1 in physiological and pathophysiological angiogenesis: applications and therapies. *Biomed Res Int*, 2015:549412.
https://doi.org/10.1155/2015/549412

Supplementary information

Figs. S1–S5